Fig. 1. The scene of PET measurements during the supine and sitting conditions.

one CVD patient. Angiographic studies revealed the cross circulation through the circle of Willis, leptomeningeal collateralization, and the border zone shift according to the definition of the St Louis group (Derdeyn et al., 1999) in all 16 patients, and coronary artery branch stenosis or occlusion in all six CVDC patients (see Table 1). The border zone shift includes the asymmetry filling of anterior or posterior cerebral artery that feeds the middle cerebral artery on the compromised side. The leptomeningeal flow in the parietal region was occasionally seen in the case of retrograde filling from the posterior cerebral artery circulation. Specifically, all the CVDC patients revealed a degree of leptomeningeal connections at the level of posterior watershed regions (middle cerebral artery and posterior cerebral artery border zone). In the two patient groups, none of the patients reported orthostatic symptoms during PET measurement. All of the patients were receiving treatment with antihypertensives, anticoagulants, and other conventional drugs for complications (see Table 1), treatment that could not be suspended before the PET scans were conducted. However, all of these medications were temporarily suspended on the day of the PET examinations. All of the patients underwent magnetic resonance imaging (MRI), which showed mild-to-moderate subcortical abnormalities (high intensities on the T2-weighted images) in the territory of the ICA on the occluded side and no involvement of the lobe infarction. The study protocol was approved by the Ethics Committee of the Hamamatsu Medical Center, and all participants gave their written informed consent after the nature and possible risks of the experiment were explained.

Postural condition and physiology

First, each participant lay calmly with his/her eyes closed on the scanner couch for approximately 40 min. After the supine condition examination was completed, the subjects were instructed to sit back against a 65° reclined (chair-like) couch with their eyes closed for about 25 min (Fig. 1). In both conditions, we recorded systemic arterial blood pressure (ABP) via a catheter placed in the brachial artery and the cardiac rhythm by electrocardiogram. Other physiological parameters, such as PaO_2, $PaCO_2$, and pH, were measured periodically. In our preliminary study, a very short-term elevation of systemic ABP after a postural shift from the supine to the sitting position was found, followed by a gradual decline to the plateau level within about 3 min. These findings were in agreement with results from

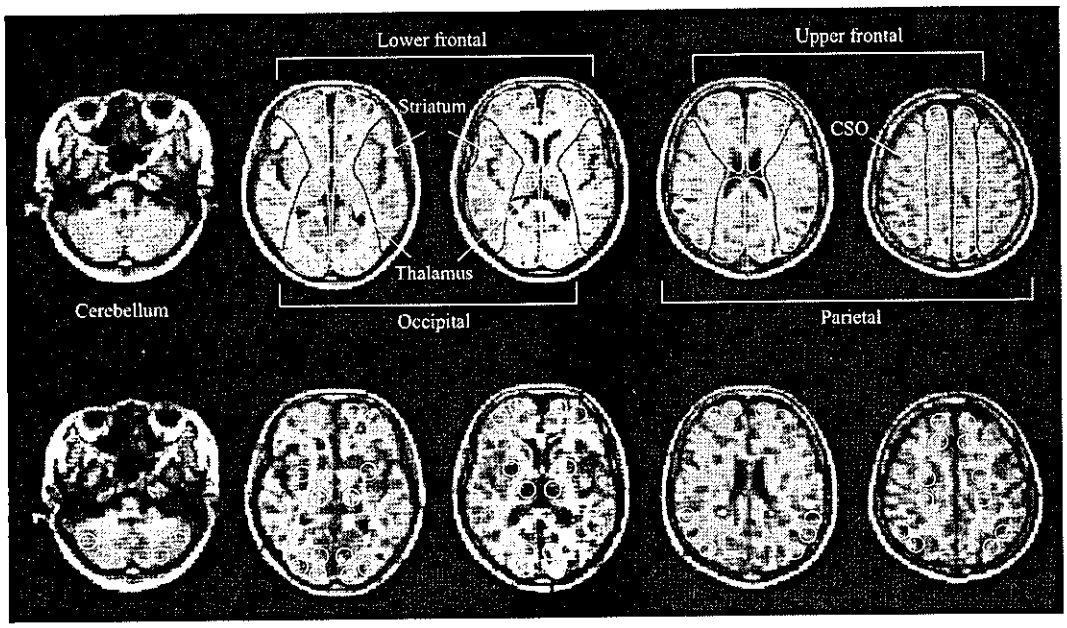

Fig. 2. ROI setting. Multiple circular ROIs consisting of 96 pixels (1.58 cm^2) were placed on the brain regions on the reformatted MR images (upper row) with the same pixel size as that of PET, which were automatically transferred onto the PET images (lower row). CSO, centrum semiovale.

a previous ultrasonic study (Novak et al., 1998). Thus, the orthostatic PET measurements in this study were performed during the static period of ABP under the head-up condition.

PET and MRI procedures

We used a state-of-the-art high-resolution brain PET scanner (SHR12000, Hamamatsu Photonics, Hamakita, Japan), the details of which have been reported elsewhere (Watanabe et al., 2002). In brief, the scanner has 24 detector rings yielding 47 slices simultaneously with a spatial resolution of 2.9 mm (full-width at half-maximum) transaxially and 3.0 mm axially and 163 mm axial field of view. After the backprojection and filtering (Hanning filter), the reconstructed image resolution became 6.0 × 6.0 × 3.2 mm full-width at half-maximum. The voxel of each reconstructed image measured 1.3 × 1.3 × 3.2 mm. This PET system has a mobile gantry system in which the gantry can move vertically 180 cm above the floor and tilt from −20° to +90° like a mechanical chair. Just prior to the PET measurements, each participant underwent an MRI for determination of the intercommissural (AC-PC) line using a static magnet with three-dimensional mode acquisition (0.3 T MRP7000AD, Hitachi, Japan) (Ouchi et al., 1998). Because the same face mask was used between the MRI and PET studies, and because the center of scan field was beforehand calibrated between the two modalities, the PET gantry was moved, and the brain was scanned parallel to the intercommissural plane according to the MRI information received.

After fixation of the head to the head holder using a radiosurgery-purpose thermoplastic face mask, a 10-min transmission scan was first performed for attenuation correction with a $^{68}Ge/^{68}Ga$ source in the supine position. Then the serial emission scans were started based on ^{15}O-oxygen bolus inhalation (Mintun et al., 1984) and ^{15}O-water bolus injection method (Herscovitch et al., 1983) and short-period $C^{15}O$ inhalation for the cerebral blood volume (CBV) data (Lammertsma and Jones, 1983; Lammertsma et al., 1987). During the scan session, the subjects inhaled 2.0 GBq $^{15}O_2$ and, for a short period of time, 1500 MBq $C^{15}O$ flowing through a tightly fitted plastic oxygen face mask attached to the subject's face. They also received 300 MBq $H_2^{15}O$ via a catheter in the right cubital vein. Data of arterial oxygen saturation (SaO_2), arterial hemoglobin (Hb), and the hematocrit values yielded the arterial oxygen content (CaO_2) by the following formula: $CaO_2 = 1.39 \times SaO_2 \times Hb$. The rCBF- and CBV-corrected OEF values were estimated on a voxel-by-voxel basis. The voxel-based $CMRO_2$ image was finally generated using the following equation: $CMRO_2 = CBF \times OEF \times CaO_2$. The arterial blood radioactivity was determined using the automated arterial blood γ-ray coincidence counter (BACC-2: Hamamatsu Photonics K.K.), which could measure arterial input data per second (Ouchi et al., 2001b). After the first session of PET scans under the supine condition was completed, the subject's head holder was temporarily removed from the receiver of the scanner's gantry, and the head was fixated again in the sitting position. Emission scans with the same protocol were performed under the sitting condition.

Data analysis and statistics

As seen in Fig. 2, we first placed multiple circular regions of interest (ROIs) with 96 pixels (1.62 cm^2) bilaterally over the cerebellar hemisphere, lower frontal area (the orbitofrontal and inferior frontal cortices [Brodmann area or BA: 10/11]), upper frontal area (middle and superior frontal cortices [BA: 6/8]), temporal [BA: 21/22], parietal [BA: 7], occipital [BA: 17/18] cortices, the striatum, the thalamus, and the centrum semiovale (CSO) on the MR images according to the human brain atlas (Mai et al., 1997; Ouchi et al., 2001b). After completion of the ROI placement, the PET images were displayed side-by-side with the MR images using an image processing system (DrView, Asahi Kasei Co, Tokyo, Japan) (Ouchi et al., 2001a,b) on a SUN workstation (Hypersparc ss-20, SUN Microsystems, CA, USA), which enabled the automatic placement of ROIs on the same area on both the MR and corresponding PET images (CBF, $CMRO_2$, OEF, CBV under both supine and sitting conditions). Quantitative data in the normal group were calculated by averaging the bilateral values in each region. The ROIs on the upper frontal and parietal region as well as the CSO were regarded as the loci for the distal part of the affected ICA territory.

For statistical analysis, baseline data collected in the supine posture were compared among the three groups by two-way analysis of variance (ANOVA) with respect to the type of group (CVD, CVDC, and Normal) and type of location, that is, occluded or non-occluded side. Since no cross-interactions were observed in the ANOVA between the two factors ($P = 0.4384$), repeated measure ANOVA was then performed to compare the parameters among groups on each hemispheric side separately. Since the perfusion territorial changes in hemodynamic param-

Table 2
Physiological data in patients with cerebrovascular disease and normal controls

Group	Condition	MABP	Pulse rate	$PaCO_2$	pH
CVD	Supine	103.2 ± 11.3*	72.3 ± 14.3	40.3 ± 3.4	7.4 ± 0.0
	Sitting	99.5 ± 14.7*	74.3 ± 14.9	40.2 ± 3.4	7.4 ± 0.0
	Change (%)	−3.36	3.10	−0.72	0.0
CVDC	Supine	95.7 ± 8.9	73.2 ± 11.6	41.1 ± 2.0	7.4 ± 0.0
	Sitting	90.8 ± 8.2	74.5 ± 8.5	40.6 ± 1.9	7.4 ± 0.0
	Change (%)	−5.1	2.5	−1.1	−0.1
NC	Supine	94.0 ± 8.0	62.4 ± 7.3	41.7 ± 2.9	7.4 ± 0.0
	Sitting	91.2 ± 8.1	65.9 ± 6.8	41.8 ± 3.5	7.4 ± 0.0
	Change (%)	−2.93	3.49	0.01	0.0

Values are expressed as mean ± SD. CVD, cerebrovascular disease (internal carotid artery occlusion or severe stenosis); CVDC, CVD with coronary artery disease; NC, normal controls; MABP, mean arterial blood pressure; Change (%), ([sitting − supine]/supine × 100) expressed as a mean value.
* $P < 0.05$ (χ^2 test) vs. normal control.

Table 3
Parameter changes by postural shift in patients with cerebrovascular disease and normal controls

Group	Parameter	State	Cerebellum		Lower frontal		Upper frontal		Parietal		Occipital		Striatum		Thalamus		CSO	
			Intact	Affected	Intact	Affected	Intact	Affected	Intact	Affected	Intact	Affected	Intact	Affected	Intact	Affected	Intact	Affected
CVD	CBF	Supine	42.6 ± 8.8	47.9 ± 9.7	40.2 ± 4.7	35.3*** ± 8.4	43.8 ± 7.0	39.3*** ± 8.7	41.5 ± 8.3	38.7*** ± 8.7	41.7 ± 9.2	41.8 ± 9.9	51.8 ± 9.9	43.8 ± 10.9	52.5 ± 10.4	48.2 ± 9.8	24.0 ± 4 5	23.9 ± 4.8
		Sitting	41.0 ± 7.9	46.8 ± 8.1	39.2 ± 6.0	34.0 ± 8.9	42.2 ± 5.6	36.6 ± 8.0	40.2 ± 8.3	35.6 ± 8.0	40.0 ± 8.7	40.1 ± 6.2	45.7 ± 9.1	36.2 ± 9.3	49.0 ± 10.1	44.8 ± 9.3	23.6 ± 4.6	22.2 ± 5.6
		%Δ	−3.28	−3.04	−3.1	−3.6	−3.48	−5.89	−2.75	−6.59***	−1.76	−1.62	−2.50	−5.12	−4.85	−6.39	−2.67	−4.83
	$CMRO_2$	Supine	3.1 ± 0.8	3.4 ± 0.9	2.7 ± 0.7	2.6 ± 0.8	3.0 ± 0.6	3.0 ± 0.7	2.7 ± 0.8	2.9 ± 0.8	2.8 ± 1.2	2.8 ± 1.1	3.3 ± 1.0	3.1 ± 1.1	3.2 ± 0.7	3.0 ± 1.2	1.1 ± 0.5	1.2 ± 0.6
		Sitting	3.3 ± 1.0	3.3 ± 0.8	2.7 ± 0.9	2.6 ± 0.8	2.6 ± 0.8	2.7 ± 0.8	2.8 ± 0.9	2.8 ± 1.0	3.1 ± 0.9	2.9 ± 1.0	2.7 ± 1.1	2.6 ± 1.0	3.0 ± 1.0	3.8 ± 1.2	1.4 ± 0.7	1.3 ± 0.6
		%Δ	3.45	2.71	2.02	2.2	3.94	3.18	5.22	2.88	3.33	4.32	−0.20	−0.26	1.12	−0.72	2.18	1.77
	OEF	Supine	39.9 ± 7.0	40.4 ± 7.8	42.0 ± 7.0	42.8*** ± 8.2	40.3 ± 5.1	40.9 ± 5.2	40.9 ± 6.1	42.4*** ± 5.6	42.6 ± 8.0	42.8 ± 8.8	40.0 ± 8.4	39.1 ± 8.4	37.2 ± 7.7	37.8 ± 8.1	32.4 ± 7.3	34.3 ± 6.2
		Sitting	43.0 ± 10.2	41.4 ± 8.4	43.1 ± 9.5	44.4 ± 9.0	41.5 ± 7.8	44.7 ± 7.2	44.1 ± 6.5	48.6 ± 7.8	43.8 ± 9.0	45.1 ± 8.7	40.3 ± 9.3	40.5 ± 9.3	38.5 ± 10.4	40.0 ± 9.8	33.0 ± 6.8	35.8 ± 5.3
		%Δ	5.06	4.74	4.10	6.22	6.97	10.81***	8.9	16.09**	4.10	6.22	4.53	5.06	4.74	6.98	7.90	6.08
	CBV	Supine	3.8 ± 0.5	4.3 ± 1.0	2.9 ± 0.5	3.0 ± 0.7	2.7 ± 0.6	2.6 ± 0.3	3.2 ± 0.7	3.6 ± 0.9	3.6 ± 0.5	4.3 ± 1.0	2.7 ± 0.4	2.6 ± 0.3	2.4 ± 0.6	3.0 ± 0.6	1.9 ± 0.4	1.9 ± 0.5
		Sitting	3.8 ± 0.8	4.7 ± 1.8	3.0 ± 0.5	3.1 ± 0.6	3.0 ± 0.3	2.8 ± 0.4	3.2 ± 0.7	3.6 ± 0.6	3.7 ± 0.4	4.1 ± 0.6	2.7 ± 0.3	2.6 ± 0.3	2.3 ± 0.3	3.9 ± 0.7	2.0 ± 0.7	1.8 ± 0.4
		%Δ	−0.55	3.01	4.78	2.39	5.8	5.08	3.52	0.78	4.52	4.13	−2.86	2.17	−0.54	3.12	0.87	0.29
CVDC	CBF	Supine	38.2 ± 0.8	42.3 ± 12.3	34.0 ± 11.0	32.5*** ± 6.1	35.5 ± 10.8	34.6 ± 9.7	35.9 ± 8.5	31.4*** ± 8.2	33.3 ± 8.4	29.9*** ± 10.4	44.9 ± 16.6	45.1 ± 12.1	43.5 ± 16.2	40.2 ± 13.5	18.3 ± 5.6	20.1 ± 6.4
		Sitting	35.4 ± 12.2	37.0 ± 11.5	33.0 ± 10.3	31.5 ± 7.3	32.2 ± 9.9	29.2 ± 7.2	31.9 ± 7.9	26.8 ± 7.7	34.0 ± 9.2	29.5 ± 9.0	39.3 ± 15.1	37.4 ± 12.7	43.6 ± 11.4	40.1 ± 10.4	18.0 ± 5.4	16.8 ± 6.7
		%Δ	−8.6	−10.5	−4.3	−3.4	−10.4	−14.7***	−12.2	−14.1*·**	−9.2	−10.3	−12.5	−15.7***	−1.6	−0.3	−1.9	- 4.1
	$CMRO_2$	Supine	2.6 ± 0.6	2.6 ± 0.7	2.4 ± 0.8	2.3 ± 0.5	2.4 ± 0.6	2.3 ± 0.5	2.4 ± 0.6	1.9** ± 0.8	2.4 ± 0.5	2.1 ± 0.9	3.2 ± 1.2	3.0 ± 0.6	2.7 ± 0.7	2.8 ± 1.1	1.1 ± 0.4	1.1 ± 0.5
		Sitting	2.8 ± 0.9	2.6 ± 0.8	2.4 ± 1.1	2.3 ± 0.5	2.3 ± 0.9	2.2 ± 0.6	2.5 ± 0.7	1.9 ± 0.9	2.3 ± 0.7	2.1 ± 1.0	2.9 ± 1.2	3.0 ± 0.5	2.7 ± 1.0	2.8 ± 1.3	0.9 ± 0.2	1.2 ± 0.6
		%Δ	7.2	1.2	−1.2	0.6	−4.4	−5.2	5.2	−7.8*·**	−5.7	−2.1	−9.3	0.1	−2.2	−1.0	−9.8	6.8
	OEF	Supine	43.1 ± 5.1	38.6 ± 5.8	42.0 ± 7.9	42.9 ± 8.1	39.3 ± 8.5	40.7 ± 9.2	40.8 ± 6.3	40.3 ± 3.5	41.6 ± 9.3	38.3 ± 10.2	43.5 ± 5.6	38.2 ± 6.1	35.4 ± 9.3	36.3 ± 7.8	28.3 ± 5.7	26.5 ± 9.0
		Sitting	46.4 ± 7.7	41.8 ± 4.0	44.4 ± 2.8	43.8 ± 6.7	42.0 ± 8.1	46.0 ± 8.6	43.5 ±	45.2 ± 3.7	46.5 ± 9.6	38.0 ± 11.2	41.4 ± 5.9	44.6 ± 8.7	31.9 ± 8.4	37.3 ± 6.9	28.0 ± 4.1	28.8 ± 8.1
		%Δ	7.4	9.2	6.6	3.5	7.7	14.1***	6.0	12.8***	11.7	6.4	−4.8	16.6	−9.0	3.5	0.1	11.3
	CBV	Supine	4.0 ± 0.8	4.5 ± 0.7	3.9 ± 4.0	3.6 ± 1.9	3.1 ± 0.6	3.1 ± 0.7	3.4 ± 0.5	3.9 ± 0.8	3.8 ± 0.6	4.5 ± 2.1	3.3 ± 1.4	3.4 ± 1.2	3.6 ± 0.8	3.0 ± 0.3	2.2 ± 0.4	2.7 ± 0.9
		Sitting	4.1 ± 0.7	4.5 ± 0.8	3.5 ± 0.7	3.5 ± 0.8	2.9 ± 0.3	3.0 ± 0.5	3.5 ± 0.6	3.5 ± 0.6	4.0 ± 0.7	4.2 ± 1.9	2.9 ± 0.7	3.2 ± 1.2	3.6 ± 0.7	3.2 ± 0.2	2.3 ± 0.6	2.5 ± 0.9
		%Δ	5.8	4.8	−10.6	−3.5	−2.2	−2.7	3.8	−4.8	5.2	−2.1	−5.9	−7.0	0.2	6.4	−1.3	−6.9
Normal	CBF	%Δ	−2.6		−4.43		−4.87		−4.92		−4.59		−5.43		−5.41		−2.58	
	$CMRO_2$	%Δ	1.51		−2.11		2.05		0.45		0.01		−0.21		−0.38		1.61	
	OEF	%Δ	3.7		5.36		5.9		5.61		5.8		5.38		5.2		5.49	
	CBV	%Δ	−1.34		3.29		1.14		4.87		4.23		−1.64		4.51		1.25	

Values are expressed as %. CVD, cerebrovascular patients (internal carotid artery occlusive disease); CVDC, internal carotid artery occlusive disease with coronary artery disease; NC, normal controls; CSO, centrum semiovale; CBF, cerebral blood flow; $CMRO_2$, cerebral metabolic rate of oxygen; OEF, oxygen extraction fraction; CBV, cerebral blood volume; %Δ: ([sitting − supine]/supine × 100).

* $P < 0.05$ vs. CVD.

** $P < 0.05$ vs. normal controls.

*** $P < 0.1$ (subsignificant) vs. normal controls.

eters (i.e., the ICA territory) were of interest, a Bonferroni post hoc test was applied within the same territory, and a P value less than 0.05 was regarded as statistically significant. Simple linear regression analyses were performed to analyze the relation between postural changes of metabolic parameters ($CMRO_2$ and OEF) and the changes of the perfusion pressure index (CBF/CBV) in the CVD and CVDC groups, separately. In addition, the postural changes in these hemodynamic parameters were compared against the changes in mean ABP in the distal ICA regions. The level of significance was also assumed as $P < 0.05$.

In addition, we added a voxel-based analysis to evaluate postural changes in rCBF more objectively between disease and healthy conditions using statistical parametric mapping (SPM) software (SPM99; Wellcome Department of Cognitive Neurology, London, UK) (Friston et al., 1995). The detail procedure was reported elsewhere (Ouchi et al., 2001a). In brief, normalized data were smoothed with an isotropic Gaussian kernel of 8 mm, resulting in the smoothed images with voxel sized of 2 × 2 × 2 mm. In the present study, however, we used quantitative CBF data for the voxel-wise analysis without analysis of covariance with global normalization. The regions with clusters of voxels over 50 and a peak height $P < 0.001$ uncorrected for multiple comparison were regarded as significant. In addition, a single-subject analysis was performed to examine individual variability. The significant level of this analysis was assumed to be $P < 0.003$ uncorrected for multiple comparison for the peak height with voxels over 50.

Results

Physiological changes

There was a tendency for postural decrease of the mean arterial blood pressure (MABP) in the CVDC group to occur, but the physiological parameters (MABP, pulse rate, $PaCO_2$, and arterial pH) were not significantly different between the supine and upright conditions among the three groups ($P > 0.05$, repeated-measures ANOVA) (Table 2). No clinical symptoms, such as hyperventilation, faintness, and syncope, were observed during the upright posture in any of the participants. Each electrocardiogram showed no significant ST-segment depression during the upright condition in the CVDC group.

ANOVA for absolute postural changes in hemodynamic and metabolic parameters

At baseline, one-way ANOVA showed significant reductions in rCBF in the parietal, frontal, and occipital cortices on the affected side and in the $rCMRO_2$ in the parietal counterpart in the CVDC group compared with the normal group ($P < 0.05$, Table 3). Repeated measures ANOVA showed significant absolute reductions in rCBF and $rCMRO_2$ in the affected-side parietal cortex in the CVDC group during upright posture compared with those in the CVD and normal groups, while rCBF (with a decrease tendency) and the $rCMRO_2$ in the area failed to show significant changes in the CVD group. The level of OEF in the affected-sided parietal cortex during sitting was significantly higher in the disease groups than that in the normal group (similar to the hemodynamic change "misery perfusion") (Baron et al., 1981). Table 4 showed mean levels of each parameter estimated for values of the territory of ICA, hemispheric, and global regions.

Relations between postural changes in oxygen metabolic parameters ($CMRO_2$, OEF) and changes in perfusion pressure index (CBF/CBV)

There were significant negative correlations of the postural changes in %ΔCBF/CBV with %ΔOEF in the upper frontal ($y = -1.38x - 6.12$, $r = 0.70$, $P < 0.05$) and parietal ($y = -1.03x - 1.73$, $r = 0.79$, $P < 0.05$) cortices and with $\%\Delta CMRO_2$ in the upper frontal ($y = -1.59x - 28.5$, $r = 0.68$, $P < 0.05$) and parietal ($y = -1.97x - 32.3$, $r = 0.73$, $P < 0.05$) cortices on the affected side in the CVDC group (Fig. 3), indicating that metabolic demand was raised as perfusion pressure decreased. In the CVD group, the postural changes in the parietal OEF tended to correlate negatively with the CBF/CBV changes ($r = 0.59$, dotted line) on the affected side, while the two parameters showed positive correlation ($r = 0.57$, dotted line) on the non-occluded side (Fig. 3D).

Relations between postural changes in hemodynamic and metabolic parameters and mean arterial blood pressure

Because the parameters varied significantly in the parietal cortex, we focused on changes in this region. In other brain regions, there was a similar tendency in the upper frontal cortex (not shown).

Table 4
Mean levels of territorial cerebral blood flow during the postural conditions (supine/sitting) in three groups

Group	Parameter	Global	Hemisphere		ICA territory	
			Intact	Affected	Intact	Affected
CVD	CBF	42.9/41.4	46.6/45.2	42.6/40.4	45.7/44.1	41.2/39.1
	CMRO	2.8/2.9	3.1/3.1	2.9/2.9	3.0/3.1	2.8/2.9
	OEF	38.9/41.0	39.4/41.3	39.8/42.5	39.6/41.8	40.2/43.3
	CBF/CBV	13.6/13.0	14.9/14.4	13.8/12.8	15.0/14.3	13.4/12.4
CVDC	CBF	35.9/33.5	37.9/36.2	35.8/33.1	35.9/34.4	34.3/31.7
	CMRO	2.33/2.41	2.6/2.6	2.4/2.4	2.4/2.5	2.3/2.2
	OEF	37.4/39.9	39.2/40.7	38.5 41.5	38.6/41.2	41.1/43.4
	CBF/CBV	10.7/10.1	11.5/10.9	10.8/10.0	10.5/10.4	10.4/9.9
NC	CBF	43.8/42.1	46.9/44.4	46.4/44.8	43.4/42.0	43.5/41.7
	CMRO	2.7/2.7	2.9/2.9	2.8/2.8	2.7/2.7	2.7/2.7
	OEF	43.8/42.2	38.6/40.4	37.0/38.3	38.7/40.0	38.0/39.4
	CBF/CBV	12.8/12.0	13.6/12.4	13.1/12.4	12.8/11.9	13.0/12.3

CBF, cerebral blood flow (ml/100 g/min); $CMRO_2$, cerebral metabolic rate of oxygen (ml/100 g/min); OEF, oxygen extraction fraction (%); CBV, cerebral blood volume (ml/100 g), CBF/CBV (%).

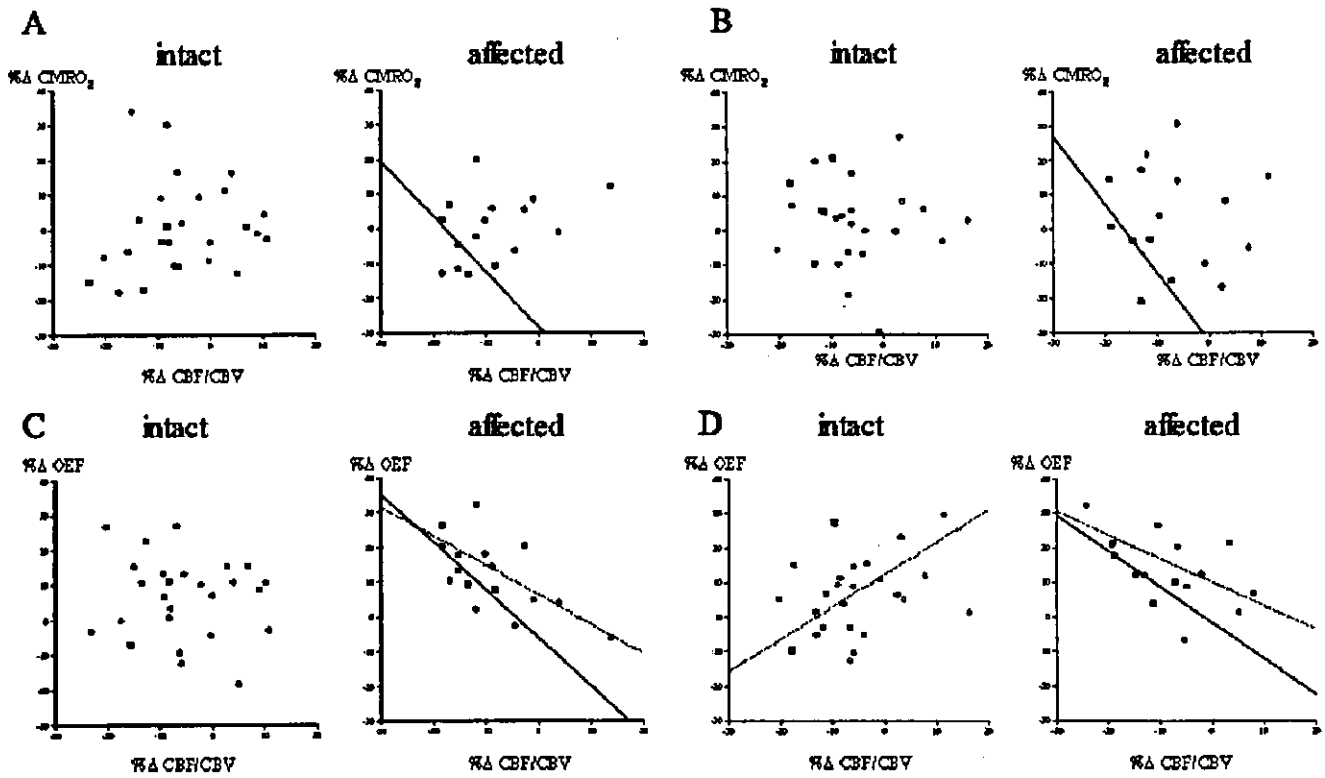

Fig. 3. Correlations between changes in perfusion pressure index (CBF/CBV) and changes in oxygen metabolism (A and B) and oxygen extraction fraction (C and D) in susceptible regions (A and C, upper frontal cortex; B and D, parietal cortex) in the normal (white circle), CVD (black circle, dotted line), and CVDC (marked square, straight line) groups. Straight lines denote significant correlations ($P < 0.05$), and dotted lines show subsignificant correlations ($P < 0.1$).

In the normal group, the values of CBF, $CMRO_2$, and OEF in the parietal cortex were almost constant with the MABP change (Figs. 4A–C, intact side, dashes). However, postural reduction in rCBF became significantly greater with MABP reduction ($y = 2.82x + 0.22$, $r = 0.80$, $P < 0.05$) in the CVDC group (Fig. 4A, affected side). Postural changes in metabolic parameters (OEF) significantly correlated negatively with MABP change ($y = -4.03x - 7.63$, $r = 0.88$, $P < 0.05$) (Fig. 4C, affected side), and so did the $CMRO_2$ change ($y = -7.07x - 40.5$, $r = 0.74$, $P < 0.05$) (Fig. 4B, affected side). In the CVD group, the rCBF change tended to correlate positively ($r = 0.60$, Fig. 4A, affected side) and the OEF change negatively ($r = 0.50$, Fig. 4C, affected side) with the MABP change.

Discussion

The present study is the first to show an absolute reduction in CBF and an increase in OEF along with a minor increase in oxygen metabolism in the hemodynamically compromised parietal region (i.e., the region more distal to the occlusion and comparable to the watershed area) in CVD patients during upright posture, suggesting the occurrence of posture-induced local neural tissue deactivation, and a further reduction in rCBF and a moderate increase in OEF along with reduced oxygen metabolism (severer deactivation) in the CVDC patients during posture (Figs. 5 and 6). Although the levels of CBV were not significantly different between postural conditions in each group, the averaged CBV values in the CVDC group tended to decrease during upright posture. The major difference between the CVD and CVDC groups was the opposite deviation in $CMRO_2$ changes in the ischemic region by a postural shift. A postural increase in OEF was commonly found in both groups, but the magnitude of the OEF increase was smaller in the CVDC group, which might cause postural reduction in $CMRO_2$. The lack of this capacity to maintain $CMRO_2$ in the CVDC group may be attributable to neuronal impairment or the scantiness of the available vascular density. It has been hypothesized that in patients with coronary artery disease, reduced flow, microemboli, and small necrosis are likely to develop due to a physical and mental stress-induced increase in blood viscosity and coagulability (Muller et al., 1989). This insidious damage in the susceptible cerebrovasculature would prevent augmentation of oxygen metabolism in the CVDC group. A greater reduction in perfusion pressure (CBF/CBV) in CVDC patients than in CVD patients might have been another explanation for the loss of metabolic increase. Taken together, upright posture may generate not only local neural deactivation in the distal part of the brain in the occluded ICA territory, but also impairment of local metabolic regulation in the area, if concomitant with cardiac ischemia. The latter problem can be a consecutive setback in the recovery of neuronal function during rehabilitation.

The postural effect on cerebral hemodynamics has been widely examined with transcranial Doppler sonography that enables the assessment of orthostatically rapid hemodynamic changes. The greater advantage of our study over sonography was the ability to quantitatively measure not only vascular, but also metabolic states in cerebrovascular regulations during assumption of the upright posture. An absolute reduction in rCBF in the hemodynamically vulnerable region under our orthostatic conditions was in line with the sonographic result showing orthostatic reduction in the perfusion velocity of intracranial large vessels (Fig. 7; Daffertshofer et al., 1991; Novak et al., 1998). As for methodological

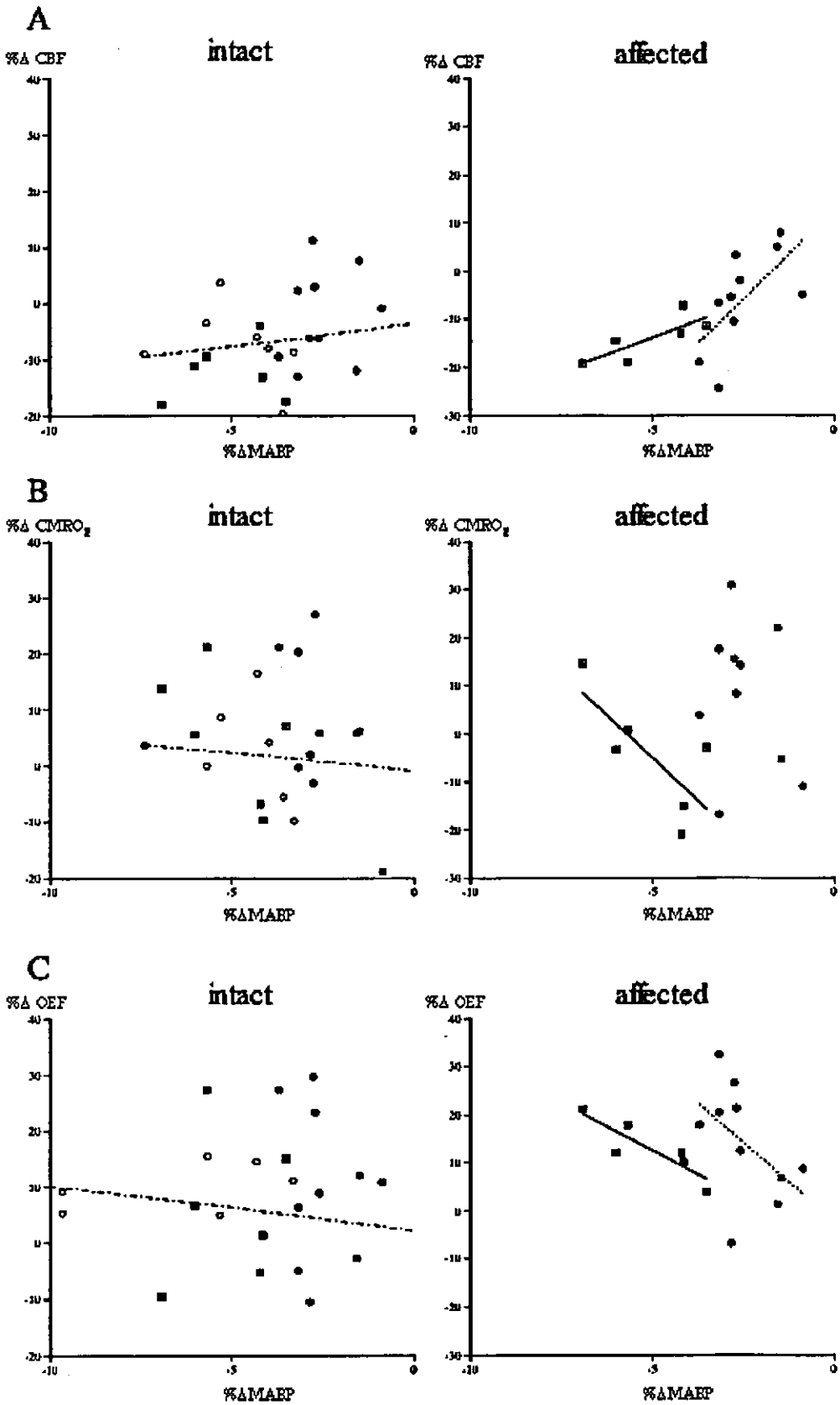

Fig. 4. Correlations of %reduction in mean arterial blood pressure (%ΔMABP) with %changes in perfusion (%ΔCBF, A), oxygen metabolism (%ΔCMRO$_2$, B), and oxygen demand index (%ΔOEF, C) in the hemodynamically vulnerable parietal region in the normal (white circle, dashes), CVD (black circle, dotted line) and CVDC (marked square, straight line) groups. While the cerebrovascular and metabolic parameters reached a plateau with the MABP change in the normal group, significant correlations were observed in the disease groups (see the Results), although the width of the MABP change was relatively small.

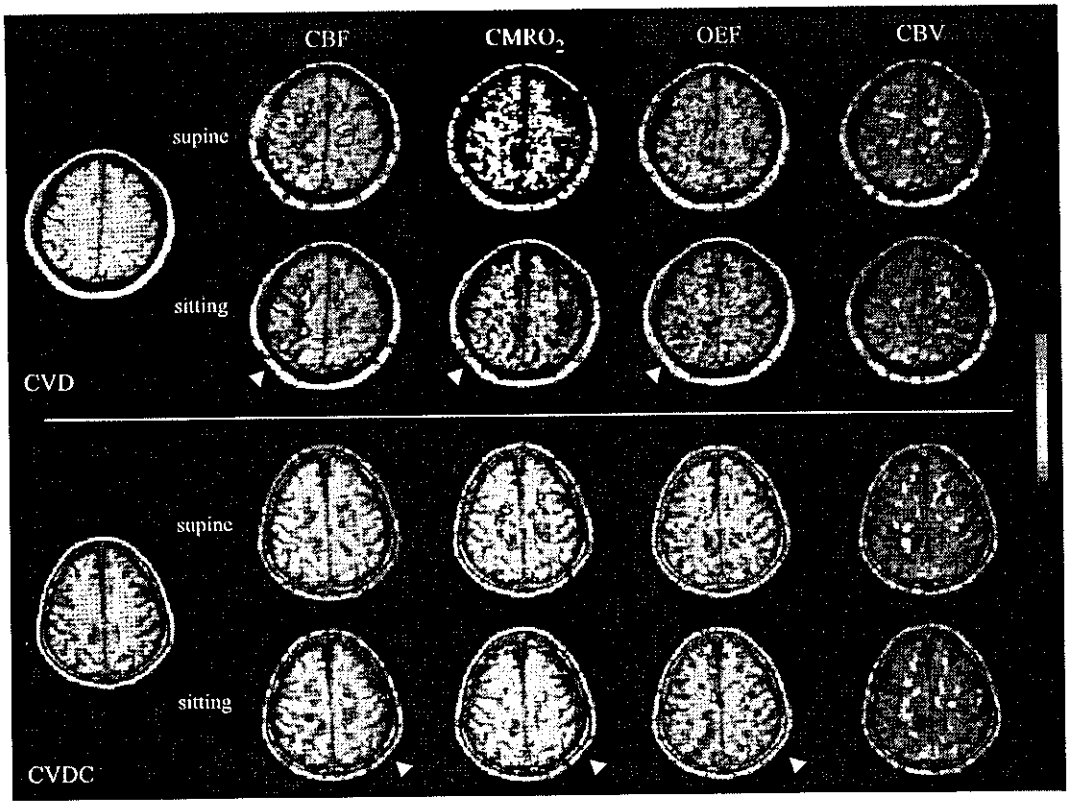

Fig. 5. PET images of a patient with right internal carotid occlusive disease (CVD) and one with left CVD plus coronary artery disease (CVDC) during supine and sitting postures. There were no abnormalities in the magnetic resonance images, but postural alterations in the hemodynamic and metabolic parameters were detected in the susceptible regions (arrowheads) in each disease group: reductions in CBF and $CMRO_2$ with slight increase in OEF in the CVDC group, and reduction in CBF with stable $CMRO_2$ and increase in OEF in the CVD group under the sitting condition.

caveats that must be taken, the timing of $CMRO_2$ acquisition was theoretically different from that of the CBF measurement in our study, and the PET data were acquired at least 15 min after the postural shift from the supine to sitting condition. These methodological limitations did not permit depiction of the dynamic phase of ongoing postural behavior and did not allow oxygen metabolism to be regarded as an independent measure from CBF, because $CMRO_2$ was quantified with the value of CBF. No significant changes in physiological parameters during the upright condition, however, could indicate the adequacy of handling CBF as a stable parameter during the upright condition, because the oxy/deoxy hemoglobin concentration reached a plateau 3 min after the

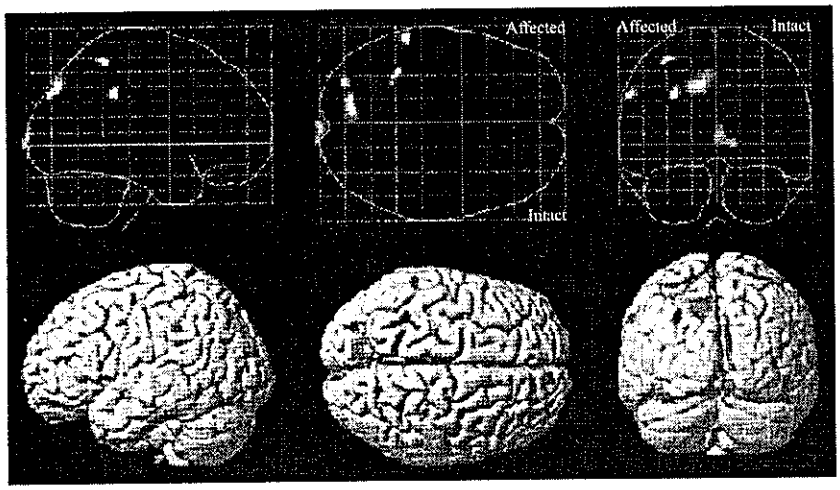

Fig. 6. SPM showed significant reduction in relative rCBF in the superior ($x\ y\ z = -34\ -46\ 60$, z score = 4.02) and inferior ($x\ y\ z = -58\ -40\ 36$, z score = 3.98) parietal lobules and precuneus ($x\ y\ z = -10\ -78\ 40$, z score = 4.38) on the occlusion side during sitting vs. lying ($P < 0.001$, uncorrected) in the disease group. The present result was similar to, but topographically different from, the previous result (Ouchi et al., 2001a,b), showing parietotemporal and frontal reductions in CBF. This discordance might be ascribed to differences in PET scanners used and in diseases analyzed (middle cerebral artery occlusion vs. ICAO).

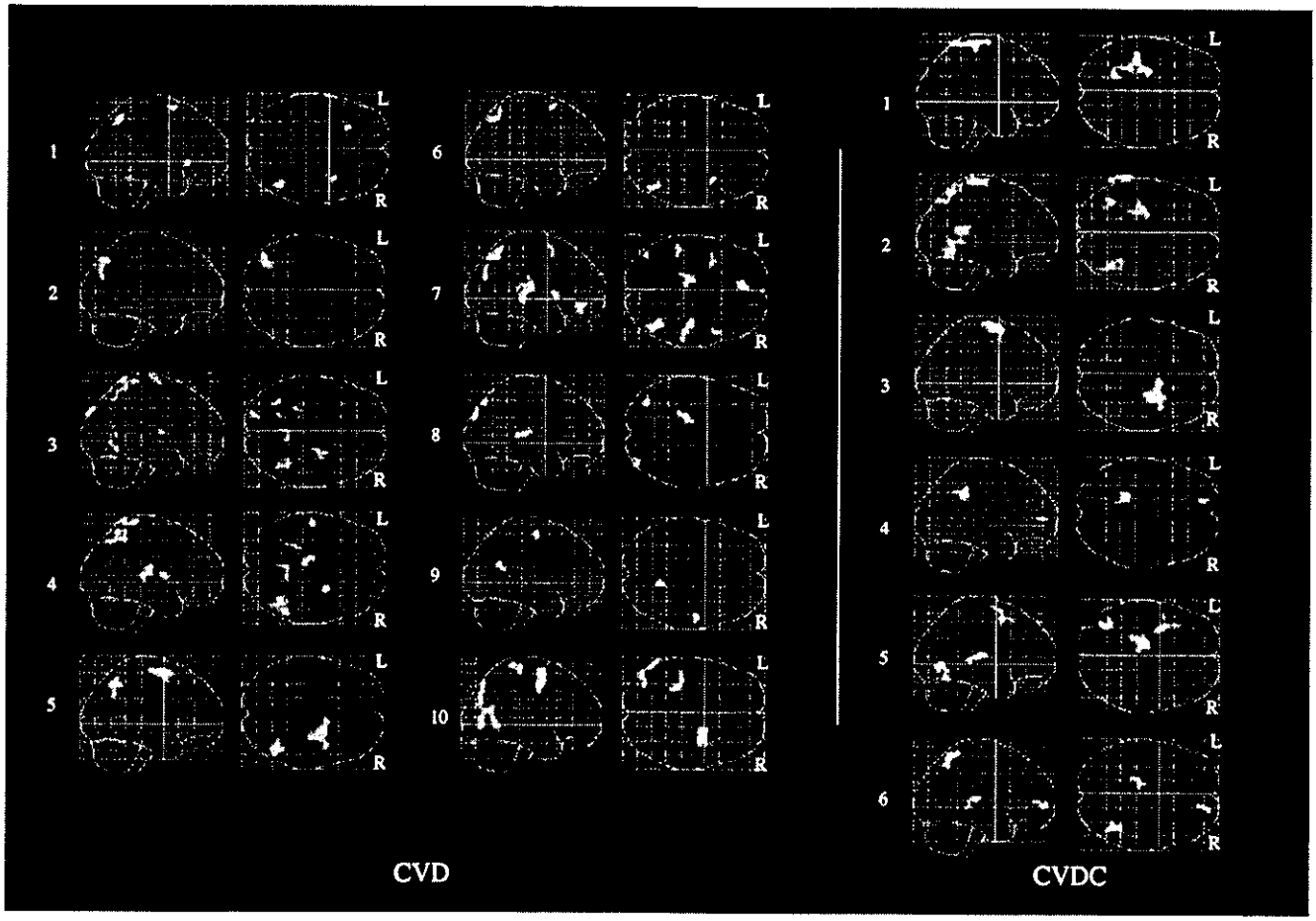

Fig. 7. Single-subject analysis for reduction in rCBF during sitting. The numbers of each glass brain correspond to the patient numbers seen in the Table 1. R, right; L, left.

postural change (Krakow et al., 2000). Although there were no significant differences in physiology among the three groups in the present study, it was not possible to determine the autonomic effect on the vasoneuronal and vasomuscular tones in the cerebral hemodynamics. Therefore, it is possible that there was a greater degree of implicit sympathetic effect that triggered a hemodynamic change in the coronary circulation (Muller, 1999) in the CVDC group, resulting in a reduction in cardiac output followed by a decrease in the cerebrovascular perfusion pressure.

The level of rCBF in the healthy group remained rather unchanged during the upright posture, which means that postural rCBF reduction might be ascribed to the impairment of local autoregulation in hemodynamically vulnerable regions in disease groups. This ABP-related CBF reduction was more significant in the affected-side parietal cortex in the CVDC group, and the relative metabolic demand was inversely augmented with MABP reduction (Fig. 4), suggesting that the susceptible ischemic region would require more energy to survive or maintain normal vasoreactivity for a further vascular dilatation event in CVD patients with cardiac ischemia. This speculation might be further supported by the present finding that a reduction in CBF/CBV correlated negatively with an increase in OEF and $CMRO_2$ in the frontal and parietal cortex distal to the affected region in the CVDC group (Fig. 3). The tendency of this negative correlation was also seen in the CVD group. In ischemic areas distal to an arterial occlusion, the arteriolar pressure has been considered to be much lower than that in the normal tissue and below the lower limit of autoregulation (Paulson, 1970; Shima et al., 1983; Symon et al., 1976). In the ischemic situation, the vascular (capillary-to-vein) pool or CBV has been considered to increase due to autoregulatory dilatation in the affected blood vessel to compensate for perfusion pressure reduction (Powers, 1991). Although a significant difference was not detected in the quantitative CBV level, due chiefly to large standard deviations (not shown) in the present study, the CBV tended to decrease in the vulnerable region during the upright posture, particularly in the CVDC group (Table 3). A recent PET study showed that acute administration of acetazolamide, a vasodilatory effect agent, resulted in an increase in the arterioler blood volume coupled with a rCBF reduction in those CVD patients with good collateral circulation (Okazawa et al., 2003). Thus, it was assumed that energy production might not be enough to make the arterioles respond to impending ischemic events when CVDC patients assume an upright posture. The lack of a decrease tendency of CBV in the CVD group might indicate that the vasodilatory capacity of arterioles in the ischemic region was sufficient.

From a clinical point of view, the incidence of ischemic stroke is at its maximum from eight to noon, the period of day during which blood pressure is at its highest in awake patients with stroke (Marler et al., 1989). The incidence of transient episodes of myocardial ischemia is also at a high point during this period (Muller, 1999). Thus, adequately controlling hypertension may be crucial for preventing the further development of stroke events for

patients when they are in an upright position. This issue is indeed important, because early introduction of active physical exercise after stroke is important for minimizing the long-term burdens of stroke (Hankey et al., 2002). During positive rehabilitation at an early stage, however, a fluctuation in neurological recovery has been reported to be occasionally encountered in patients with cardiovascular problems (Dromerick and Reding, 1994). In addition, acute recovery from cerebral ischemic attack was not considered a good sign, but, rather, an impending omen of subsequent neurological deterioration (Johnston et al., 2003). The present orthostatic PET measurement could provide one insight into the mechanism by which neurological deterioration on a molecular level develops in the susceptible brain region. However, the small sample size in the CVDC group would require a more extensive study for a number of patients with cardiac problems (symptomatic or asymptomatic), and hence the present result should be considered preliminary at this stage.

In conclusion, the current study demonstrated that upright posture caused local neural deactivation in the hemodynamically vulnerable brain region in patients with CVD. When the cardiac problem is accompanied by a CVD condition, the tissue oxygen demand would be increased with a decrease in perfusion pressure in the hemodynamically susceptible region, but a sufficient degree of net energy production might not be expected during the upright posture. The proper control of hypertension or drinking adequate amounts of water (Schroeder et al., 2002; Shannon et al., 2002) can reduce this insidious menace in CVD patients in general.

Acknowledgments

We would like to thank Dr. Teiji Nakyama, Dr. Masanobu Sakamoto, Dr. Kenichi Yano, Mr. Fumitoshi Nakamura, Ms. Tomomi Ogusu, and other staff in the Positron Medical Center for their advice and support on PET measurements. This study was supported by a grant from the Takeda Science Foundation.

References

Baron, J.C., Bousser, M.G., Rey, A., Guillard, A., Comar, D., Castaigne, P., 1981. Reversal of focal "misery-perfusion syndrome" by extra intracranial arterial bypass in hemodynamic cerebral ischemia. A case study with 15O positron emission tomography. Stroke 12, 454–459.

Daffertshofer, M., Diehl, R.R., Ziems, G.U., Hennerici, M., 1991. Orthostatic changes of cerebral blood flow velocity in patients with autonomic dysfunction. J. Neurol. Sci. 104, 32–38.

Derdeyn, C.P., Shaibani, A., Moran, C.J., Cross III, D.T., Grubb Jr., R.L., Powers, W.J., 1999. Lack of correlation between pattern of collateralization and misery perfusion in patients with carotid occlusion. Stroke 30, 1025–1032.

Dromerick, A., Reding, M., 1994. Medical and neurological complications during inpatient stroke rehabilitation. Stroke 25, 358–361.

Friston, K.J., Holmes, A.P., Worsley, K.J., Poline, J.P., Frith, C.D., Frackowiak, R.S.J., 1995. Statistical parametric mapping in functional imaging: a general linear approach. Hum. Brain Mapp. 2, 189–210.

Graafmans, W.C., Ooms, M.E., Hofstee, H.M., Bezemer, P.D., Bouter, L.M., Lips, P., 1996. Falls in the elderly: a prospective study of risk factors and risk profiles. Am. J. Epidemiol. 143, 1129–1136.

Hamar, J., Kovach, A.G., Reivich, M., Nyary, I., Durity, F., 1979. Effect of phenoxybenzamine on cerebral blood flow and metabolism in the baboon during hemorrhagic shock. Stroke 10, 401–407.

Hankey, G.J., Jamrozik, K., Broadhurst, R.J., Forbes, S., Anderson, C.S., 2002. Long-term disability after first-ever stroke and related prognostic factors in the Perth Community Stroke Study, 1989–1990. Stroke 33, 1034–1040.

Hayashida, K., Hirose, Y., Kaminaga, T., Ishida, Y., Imakita, S., Takamiya, M., et al., 1993. Detection of postural cerebral hypoperfusion with technetium-99 m-HMPAO brain SPECT in patients with cerebrovascular disease. J. Nucl. Med. 34, 1931–1935.

Herscovitch, P., Markham, J., Raichle, M.E., 1983. Brain blood flow measured with intravenous H215O. I. Theory and error analysis. J. Nucl. Med. 24, 782–789.

Johnston, S.C., Leira, E.C., Hansen, M.D., Adams, H.P.J., 2003. Early recovery after cerebral ischemia risk of subsequent neurological deterioration. Ann. Neurol. 54, 439–444.

Kapoor, W.N., 2000. Syncope. N. Engl. J. Med. 343, 1856–1862.

Krakow, K., Ries, S., Daffertshofer, M., Hennerici, M., 2000. Simultaneous assessment of brain tissue oxygenation and cerebral perfusion during orthostatic stress. Eur. Neurol. 43, 39–46.

Lakka, T.A., Salonen, R., Kaplan, G.A., Salonen, J.T., 1999. Blood pressure and the progression of carotid atherosclerosis in middle-aged men. Hypertension 34, 51–56.

Lammertsma, A.A., Jones, T., 1983. Correction for the presence of intravascular oxygen-15 in the steady-state technique for measuring regional oxygen extraction ratio in the brain: 1. Description of the method. J. Cereb. Blood Flow Metab. 3, 416–424.

Lammertsma, A.A., Baron, J.C., Jones, T., 1987. Correction for intravascular activity in the oxygen-15 steady-state technique is independent of the regional hematocrit. J. Cereb. Blood Flow Metab. 7, 372–374.

Levine, B.D., Giller, C.A., Lane, L.D., Buckey, J.C., Blomqvist, C.G., 1994. Cerebral versus systemic hemodynamics during graded orthostatic stress in humans. Circulation 90, 298–306.

Lipsitz, L.A., 1989. Orthostatic hypotension in the elderly. N. Engl. J. Med. 321, 952–957.

Mai, J.K., Assheuer, J., Paxinos, G., 1997. Atlas of the Human Brain. Academic Press, San Diego.

Marler, J.R., Price, T.R., Clark, G.L., Muller, J.E., Robertson, T., Mohr, J.P., et al. 1989. Morning increase in onset of ischemic stroke. Stroke 20, 473–476.

Mehagnoul-Schipper, D.J., Vloet, L.C., Colier, W.N., Hoefnagels, W.H., Jansen, R.W., 2000. Cerebral oxygenation declines in healthy elderly subjects in response to assuming the upright position. Stroke 31, 1615–1620.

Mintun, M.A., Raichle, M.E., Martin, W.R., Herscovitch, P., 1984. Brain oxygen utilization measured with O-15 radiotracers and positron emission tomography. J. Nucl. Med. 25, 177–187.

Muller, J.E., 1999. Circadian variation and triggering of acute coronary events. Am. Heart J. 137, S1–S8.

Muller, J.E., Tofler, G.H., Stone, P.H., 1989. Circadian variation and triggers of onset of acute cardiovascular disease. Circulation 79, 733–743.

Novak, V., Novak, P., Spies, J.M., Low, P.A., 1998. Autoregulation of cerebral blood flow in orthostatic hypotension. Stroke 29, 104–111.

Okazawa, H., Yamauchi, H., Sugimoto, K., Takahashi, M., 2003. Differences in vasodilatory capacity and changes in cerebral blood flow induced by acetazolamide in patients with cerebrovascular disease. J. Nucl. Med. 44, 1371–1378.

Ouchi, Y., Nobezawa, S., Okada, H., Yoshikawa, E., Futatsubashi, M., Kaneko, M., 1998. Altered glucose metabolism in the hippocampal head in memory impairment. Neurology 51, 136–142.

Ouchi, Y., Nobezawa, S., Yoshikawa, E., Futatsubashi, M., Kanno, T., Okada, H., et al., 2001a. Postural effects on brain hemodynamics in unilateral cerebral artery occlusive disease: a positron emission tomography study. J. Cereb. Blood Flow Metab. 21, 1058–1066.

Ouchi, Y., Okada, H., Yoshikawa, E., Futatsubashi, M., Nobezawa, S., 2001b. Absolute changes in regional cerebral blood flow in association with upright posture in humans: an orthostatic PET study. J. Nucl. Med. 42, 707–712.

Paulson, O.B., 1970. Regional cerebral blood flow in apoplexy due to occlusion of the middle cerebral artery. Neurology 20, 63–77.

Pitzalis, M., Massari, F., Guida, P., Iacoviello, M., Mastropasqua, F., Rizzon, B., et al., 2002. Shortened head-up tilting test guided by systolic pressure reductions in neurocardiogenic syncope. Circulation 105, 146–148.

Powers, W.J., 1991. Cerebral hemodynamics in ischemic cerebrovascular disease. Ann. Neurol. 29, 231–240.

Raiha, I., Luutonen, S., Piha, J., Seppanen, A., Toikka, T., Sourander, L., 1995. Prevalence, predisposing factors, and prognostic importance of postural hypotension. Arch. Intern. Med. 155, 930–935.

Schondorf, R., Benoit, J., Wein, T., 1997. Cerebrovascular and cardiovascular measurements during neurally mediated syncope induced by head-up tilt. Stroke 28, 1564–1568.

Schroeder, C., Bush, V.E., Norcliffe, L.J., Luft, F.C., Tank, J., Jordan, J., et al., 2002. Water drinking acutely improves orthostatic tolerance in healthy subjects. Circulation 106, 2806–2811.

Shannon, J.R., Diedrich, A., Biaggioni, I., Tank, J., Robertson, R.M., Robertson, D., et al., 2002. Water drinking as a treatment for orthostatic syndromes. Am. J. Med. 112, 355–360.

Shima, T., Hossmann, K.A., Date, H., 1983. Pial arterial pressure in cats following middle cerebral artery occlusion. 1. Relationship to blood flow, regulation of blood flow and electrophysiological function. Stroke 14, 713–719.

Strandgaard, S., Paulson, O.B., 1989. Cerebral blood flow and its pathophysiology in hypertension. Am. J. Hypertens. 2, 486–492.

Symon, L., Branston, N.M., Strong, A.J., 1976. Autoregulation in acute focal ischemia. An experimental study. Stroke 7, 547–554.

Warkentin, S., Passant, U., Minthon, L., Karlson, S., Edvinsson, L., Faldt, R., et al., 1992. Redistribution of blood flow in the cerebral cortex of normal subjects during head-up postural change. Clinic. Auton. Res. 2, 119–124.

Watanabe, M., Shimizu, K., Omura, T., Takahashi, M., Kosugi, T., Yoshikawa, E., et al., 2002. A new high resolution PET scanner dedicated to brain research. IEEE Trans. Nucl. Sci. 49, 634–639.

Yamauchi, H., Fukuyama, H., Kimura, J., Konishi, J., Kameyama, M., 1990. Hemodynamics in internal carotid artery occlusion examined by positron emission tomography. Stroke 21, 1400–1406.

ORIGINAL ARTICLES

Microglial Activation and Dopamine Terminal Loss in Early Parkinson's Disease

Yasuomi Ouchi, MD, PhD,[1] Etsuji Yoshikawa, BA,[2] Yoshimoto Sekine, MD, PhD,[1,2]
Masami Futatsubashi, BA,[2] Toshihiko Kanno, RT,[1] Tomomi Ogusu, MA,[2] Tatsuo Torizuka, MD, PhD[1]

Neuroinflammatory glial response may contribute to degenerative processes in Parkinson's disease (PD). To investigate changes in microglial activity associated with changes in the presynaptic dopamine transporter density in the PD brain in vivo, we studied 10 early-stage drug-naive PD patients twice using positron emission tomography with a radiotracer for activated microglia [^{11}C](*R*)-PK11195 and a dopamine transporter marker [^{11}C]CFT. Quantitative levels of binding potentials (BPs) of [^{11}C](*R*)-PK11195 and [^{11}C]CFT in the nigrostriatal pathway were estimated by compartment analyses. The levels of [^{11}C](*R*)-PK11195 BP in the midbrain contralateral to the clinically affected side were significantly higher in PD than that in 10 age-matched healthy subjects. The midbrain [^{11}C](*R*)-PK11195 BP levels significantly correlated inversely with [^{11}C]CFT BP in the putamen and correlated positively with the motor severity assessed by the Unified Parkinson's Disease Rating Scale in PD. In healthy subjects, the [^{11}C](*R*)-PK11195 BP in the thalamus and midbrain showed an age-dependent increase. In vivo demonstration of parallel changes in microglial activation and corresponding dopaminergic terminal loss in the affected nigrostriatal pathway in early PD supports that neuroinflammatory responses by intrinsic microglia contribute significantly to the progressive degeneration process of the disease and suggests the importance of early therapeutic intervention with neuroprotective drugs.

Ann Neurol 2005;57:168–175

The histopathological hallmarks of Parkinson's disease (PD) are the progressive degeneration of the nigral dopamine neurons and the ensuing loss of dopamine nerve terminals in the striatum.[1] Previous ex vivo and animal studies suggest that the loss of dopamine neurons is linked with an activation of microglia in the substantia nigra.[2–9] Neuropathological studies with 1-methyl-4-phenyl-1,2,3,6-tetrahydropyridine indicated that microglia might contribute to later and ongoing degeneration of nigral neurons.[10,11] Although these postmortem and animal studies have strongly suggested the relevance of microglial activation to the nigral cell death seen in PD patients, the antemortem relation between microglial expression and progressive loss of dopamine terminals in PD patients at an early stage remains unclear.

Microglia are involved in immune surveillance in the intact brain and become activated in response to inflammation, trauma, ischemia, tumor, and neurodegeneration.[12] A PD rat model with striatal lesions by 6-hydroxydopamine, secondarily causing retrograde damage to the nigral dopamine neurons, showed an increase in the binding of a specific marker for activated microglia, (1-(2-chrorophynyl)-*N*-methylpropyl)-3 isoquinoline carboxamide ([^{11}C]PK11195)[13,14] in the striatum and substantia nigra, which indicated an inflammatory response resulting from neural injury and/or neuronal death.[15] Based on use of the [^{11}C](*R*)-PK11195 enantiomer and positron emission tomography (PET), more detailed measurement of microglial activation in vivo recently has been reported in neurodegenerative disorders.[16,17] Furthermore, one of the dopamine transporter (DAT) markers, [^{11}C]2-B-carbomethoxy-3B-(4-fluorophenyl) tropane ([^{11}C]CFT), which allows us to depict the density of the dopaminergic terminals in PD patients in vivo, has shown a marked reduction in [^{11}C]CFT binding in the striatum in parallel with the severity of parkinsonism.[18–20] These in vivo imaging methods are advantageous in monitoring double aspects of progressively degenerated dopamine neurons, namely, alterations in neuroinflammatory reactions on the cell-body side and the resulting deletion of nerve terminals in the striatum.

For this purpose, we quantitatively measured the binding potentials (BPs) of [^{11}C](*R*)-PK11195 and [^{11}C]CFT in drug-naive patients with PD at an early stage on the same day because any delay in the measurement of the two tracers could obscure the accurate

From the [1]Positron Medical Center, Hamamatsu Medical Center; and [2]Central Research Laboratory, Hamamatsu Photonics K.K., Hamakita, Japan.

Received May 17, 2004, and in revised form Aug 13 and Oct 7. Accepted for publication Oct 7, 2004.

Published online Jan 26, 2005, in Wiley InterScience (www.interscience.wiley.com). DOI: 10.1002/ana.20338

Address correspondence to Dr Ouchi, Positron Medical Center, Hamamatsu Medical Center, 5000 Hirakuchi, Hamakita 434-0041, Japan. E-mail: ouchi@pmc.hmedc.or.jp

relation of ongoing neuroinflammation with neurodegeneration in the living brain.

Subjects and Methods

Participants

Ten drug-naive patients with PD rated at stage 1 to 2 on the Hoehn and Yahr scale (PD group, four men, six women; mean age, 59.6 years ± 9.9 standard deviation [SD]; range, 43–72) and 10 age-matched healthy subjects (N group, four men, six women; mean age, 53.1 years ± 12.5 SD; range, 39–70) participated in the present study. Patients who had been suffering from limb tremor, rigidity, and bradykinesia with a tentative clinical diagnosis as PD were recruited from our head hospital or the neighboring clinics, and the controls who were healthy physically and neurologically without any medication or complications were recruited by in-house advertisement. All participants underwent magnetic resonance imaging (MRI) and neurological and blood tests to exclude the possibility of any accompanying diseases. Diagnostic L-dopa treatment (L-dopa 100mg/day for 2–5 days) for all PD patients after PET examination markedly ameliorated their parkinsonian symptoms (reduction in frequency of tremor or disappearance of rigidity and bradykinesia). Clinical characteristics of PD patient are shown in Table 1. This study was approved by the ethics committee of the Hamamatsu Medical Center, and written informed consent was obtained from all participants after full explanation of the nature of the study.

Magnetic Resonance Imaging and Positron Emission Tomography Imaging

First, all participants underwent three-dimensional MRI just before the PET measurement. Here, we used a static magnet (0.3 T MRP7000AD; Hitachi, Tokyo, Japan) with three-dimensional mode sampling to determine the areas of the midbrain and the striatal nuclei required for setting the regions of interest (ROIs). The MRI measures and a mobile PET gantry allowed us to reconstruct PET images parallel to the intercommisural (anterior commissure–posterior commissure) line without reslicing; using this approach, we were able to allocate ROIs on the target regions of original PET images.[20]

PET scans were conducted with a high-resolution brain-purpose SHR12000 (Hamamatsu Photonics K.K., Hamamatsu, Japan) tomograph (intrinsic resolution, 2.9 × 2.9 ×3.4 full-width half-maximum [FWHM], 47 slices, 163mm axial field of view).[21] After the head fixation by a thermoplastic facemask and a 10-minute transmission scan for attenuation correction, serial scans (time frames: 4 × 30 seconds, 20 × 60 seconds, 14× 300 seconds) and periodical arterial blood sampling were performed for 92 minutes after a slow bolus injection (taking 1 minute) of a 350MBq dose of [^{11}C]CFT.[20,22] The [^{11}C](*R*)-PK11195 PET measurement then was performed after a 3-hour interval to allow for the decay of radioactivity. After the head was fixated at the same position as in the [^{11}C]CFT study, dynamic PET scans (4 × 30 seconds, 20 × 60 seconds, 8 × 300 seconds) were performed for 62 minutes without arterial blood sampling after intravenous injection of a 300MBq dose of [^{11}C](*R*)-PK11195.[14] The chronological order of the two PET studies was counterbalanced among the groups.

Image Data Analysis

Because gliosis is associated with changes in tissue volume,[16] a morphological study was first performed based on the previous volumetric MRI studies for midbrain morphology by measuring the maximum anteroposterior diameter of the midbrain through the substantia nigra and the maximum interpeduncular distance at the level of the substantia nigra and red nucleus on the MRIs.[23] Then, multiple semicircular ROIs (36~120mm^2) were drawn bilaterally over the midbrain (covering the substantia nigra, ventral tegmental area, and red nucleus), nucleus accumbens, ventromedial striatum (head of the caudate), the inferolateral (ventral putamen) and superodorsal parts (dorsal putamen) of the striatum, the thalamus, and the cerebellum on the MRIs.[24] These ROIs then were transferred onto the corresponding dynamic [^{11}C]CFT images and parametric images of [^{11}C](*R*)-PK11195 BP with 6.8mm slice-thickness data generated after adding two consecutive slices using image-processing software (Dr View;

Table 1. Clinical Characteristics of Parkinson's Disease Patients

Patient No.	Age (yr)	Sex	DD (yr)	H&Y	MMSE	UPDRS (me/act/mo)	Medication
1	56	M	1.6	2	29	4/4/10	Naive
2	43	M	0.9	1	29	2/4/5	Naive
3	65	M	0.8	2	29	3/6/9	Hypnotic/naive
4	72	M	1.8	2	29	4/6/11	Hypnotic/naive
5	58	F	2.5	1	30	2/4/6	Naive
6	70	F	1.2	1	27	3/8/15	Naive
7	57	F	1.9	2	27	3/6/20	Naive
8	71	F	0.9	1	29	3/4/8	Hypnotic/naive
9	48	F	0.4	1	28	2/5/9	Naive
10	56	F	1.9	2	26	4/12/11	Naive

Hypnotic medicines were temporarily used and stopped at least 1 week before position omission tomography measurement.
DD = disease duration; H&Y = modified Hoehn & Yahr disability score (1–5); MMSE = Mini-Mental State Examination (maximum = 30); UPDRS = Unified Parkinson's Disease Rating Scale (me = mentation, behavior, and mood; act = activities of daily living; mo = motor examination).

Asahi Kasei, Tokyo, Japan) on a SUN workstation (Hypersparc ss-20; SUN Microsystems, San Diego, CA).[25] The values of bilateral ROIs in the midbrain and cerebellum were averaged for further analysis.

[^{11}C](*R*)-PK11195 BP parametric images were generated according to the basis-function theory based on a simplified reference tissue model.[14,26] In this procedure, a normalized input curve was first created by averaging the ROIs placed over the cerebral cortical regions including the frontal, parietal, and occipital cortices in the healthy group. Then, we used this normalized mean tissue activity curve as the reference input function according to the cluster analysis theory[27] because a desirable reference region free of specific binding is not present in degenerative disorders, including PD. The population reference input curve (Fig 1, open circle) was used as the time activity curve (TAC) for the reference region. When applying this curve to the individual PD subjects, the normalized curve was calibrated by adjusting the cerebellar TAC peak from each PD patient. Instead of using the cluster segregation method,[14] the extracerebral structures were masked by demarcating cerebral regions on MRIs for further ROI analyses of PET images. Because, as described above, participants were scanned in the same position between the two PET measurements, the same ROIs could be placed on both [^{11}C]CFT and [^{11}C](*R*)-PK11195 parametric images. This approach allowed us to examine microglial activation in parallel with the degeneration of the presynaptic terminals in vivo. The binding potential (a ratio of binding and dissociation rate constants, k_3/k_4) for [^{11}C]CFT was analyzed based on the three-compartment model, as described elsewhere.[20,22]

Statistics

For between-group comparisons of [^{11}C]CFT and [^{11}C](*R*)-PK11195 binding levels, two-way analysis of variance (ANOVA) first was performed to assess BP levels with respect to one intersubject factor and the intrasubject factor (hemispheric side of the striatum) for evaluating the interhemispheric effect due to clinical manifestation of laterality in early PD. Because there was no significant interaction in the two-way ANOVA between the hemispheric side and types of groups ($p = 0.082$), all estimates were separately evaluated by one-way ANOVA in either region with Bonferroni's test for the correction of multiple comparisons. Statistical significance was given as p value less than 0.05 because the post hoc multiple comparisons were performed in these analyses. We previously have reported declines in [^{11}C]CFT binding associated with increases in age and in the severity of motor functions[20]; as such, simple linear regression analysis also was performed between age and [^{11}C](*R*)-PK11195 binding. In addition, Spearman's rank correlation analysis was performed to compare clinical motor scores of the Unified Parkinson's Disease Rating Scale with [^{11}C](*R*)-PK11195 binding levels in each region. The multiple regression analyses between regional [^{11}C]CFT binding and [^{11}C](*R*)-PK11195 binding were performed within each group. The level of significance was assumed to be p value less than 0.05.

Results

The Levels of [^{11}C]CFT and [^{11}C](R)-PK11195 Binding

The tissue TACs of [^{11}C](*R*)-PK11195 are shown in Figure 1. After administration of [^{11}C](*R*)-PK11195, the radioactivity in the midbrain and striatum of a healthy subject declined with time in the same fashion as the normalized mean TAC (population input curve) (see Fig 1A). In contrast, TAC of the midbrain in a

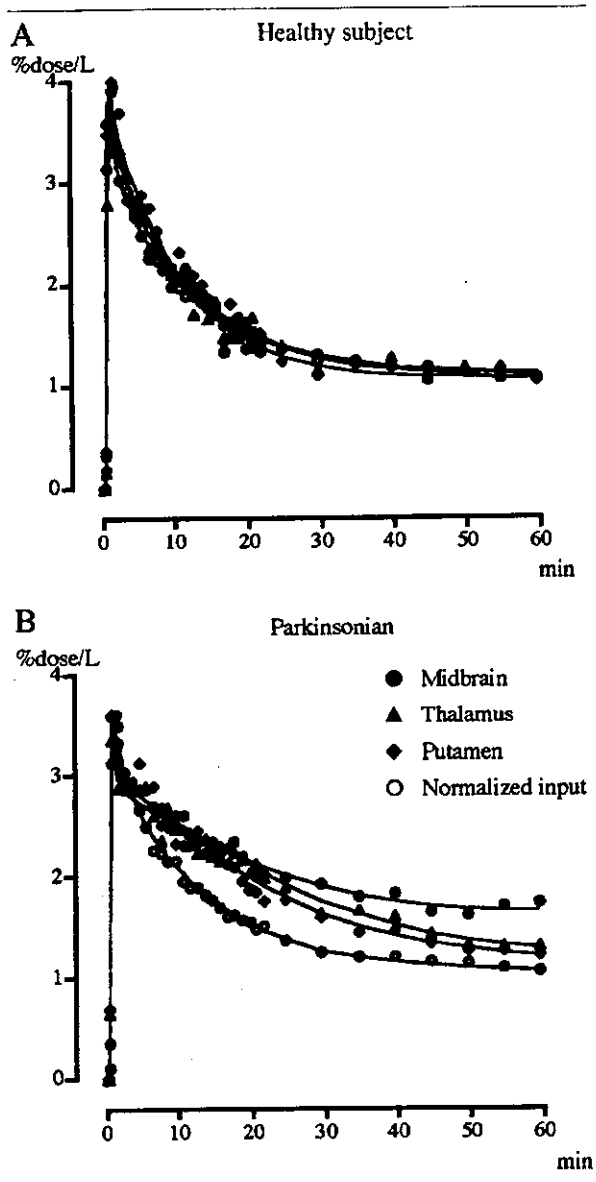

Fig 1. Regional tissue time-activity curves of [^{11}C](R)-PK11195 in a healthy subject (A) and a patient with Parkinson's disease (B). The normalized curve was generated as a reference input curve averaged from all the regions of interest values in the cerebral cortical regions without the midbrain, thalamus, and putamen in the healthy group.

Table 2. Levels of Binding Potential (k_3/k_4) for [^{11}C]CFT and [^{11}C]PK11195, Mean (SD)

Group	Tracer	DV_{CFT} $R1_{PK}$ (Bilateral)	Midbrain Bilateral	k_3/k_4 Nucleus Accumbens Ipsilateral	Nucleus Accumbens Contralateral	Caudate Ipsilateral	Caudate Contralateral	Ventral Putamen Ipsilateral	Ventral Putamen Contralateral	Dorsal Putamen Ipsilateral	Dorsal Putamen Contralateral	Thalamus Ipsilateral	Thalamus Contralateral
PD	CFT	7.86 (1.01)	ND	2.52 (0.97)	1.93*(0.58)	2.37 (0.86)	2.04*(0.85)	1.34*(0.33)	1.18*(0.27)	1.21*(0.35)	0.83*(0.24)	ND	ND
	PK	0.79 (0.06)	0.35*(0.06)	<0.01	<0.01	0.08 (0.05)	0.01 (0.01)	0.04 (0.03)	0.03 (0.02)	<0.01	<0.01	0.12 (0.06)	0.13 (0.07)
N	CFT	7.95 (0.78)	—	2.95 (0.47)		3.92 (1.13)		4.44 (1.24)		3.64 (0.82)		ND	
	PK	0.74 (0.29)	0.11 (0.06)	0.06 (0.05)		0.04 (0.04)		0.07 (0.05)		0.06 (0.04)		0.10 (0.04)	

DV_{CFT} = distribution volume for the cerebellum in the [^{11}C]CFT measurement; $R1_{PK}$ = delivery index for the midbrain in the [^{11}C]PK11195 measurement; ND denotes not determined because of the negligible accumulation of [^{11}C]CFT.

*$p < 0.05$ vs normal group.

PD patient declined less sharply, indicating a time-course accumulation of [^{11}C](*R*)-PK11195 in the midbrain (see Fig 1B, closed circle). The statistics showed that midbrain values were significantly different from those of the thalamus and putamen after 40 minutes.

One-way ANOVA showed that the levels of k_3/k_4 for [^{11}C]CFT were significantly lower in all parts of the striatum ($p < 0.01$) in the PD group than those in the healthy group. The magnitude of k_3/k_4 in the PD group was lower in the dorsal putamen contralateral to the clinically more affected side (Table 2). No differences in distribution volume (DV) in the cerebellum of [^{11}C]CFT was found between the two groups. In the [^{11}C](*R*)-PK11195 study, the BP of the tracer was greater in the midbrain of the PD group than in the healthy counterparts (see Table 2), whereas there was no difference in the ratio of delivery (R_1) of the tracer between the target (midbrain) and reference tissue between the groups. The thalamus or striatum in PD failed to show any significant difference in binding. Morphometric measurement showed no significant differences in midbrain size (anteroposterior and transverse distances) between groups (Table 3), indicating no significant partial volume effect in further tracer analyses.

Correlations of [^{11}C](R)-PK11195 Binding with Age and Motor Severity in Parkinson's Disease Patients

Levels of [^{11}C](*R*)-PK11195 binding in the midbrain of the healthy group significantly correlated positively with age ($r = 0.68$; $p < 0.05$, f[x] = 0.0035*x − 0.073), whereas no such correlation was observed in the PD group (Fig 2A). This midbrain [^{11}C](*R*)-PK11195 binding in the PD group significantly correlated positively with the motor severity of the UPRDS assessment ($r = 0.74$; $p < 0.05$, f[x] = 0.012*x + 0.19; see Fig 2B) but failed to show a significant correlation against the disease duration ($r = 0.36$, $p > 0.1$; see Fig 2C). The examined brain regions other than the midbrain showed no significant correlation between [^{11}C](*R*)-PK11195 binding and motor scores in either group (not shown).

Comparison between Binding Levels of Striatal [^{11}C]CFT and Midbrain [^{11}C](R)-PK11195 in Parkinson's Disease Patients

Regression analyses showed that estimates for [^{11}C](*R*)-PK11195 binding in the midbrain significantly correlated negatively with those for [^{11}C]CFT binding in the dorsal putamen contralateral to the affected side ($r = 0.894$; $p < 0.01$, f[x] = −4.18*x + 2.30) and its ipsilateral counterpart ($r = 0.72$, $p < 0.05$, f(x)= −3.94*x + 2.59; Fig 3C). There was a tendency toward a negative correlation in the caudate ($p > 0.05$; see Fig 3A).

Discussion

Theses results showed to our knowledge for the first time with PET markers a higher accumulation of [^{11}C](*R*)-PK11195 in the midbrain in drug-naive early PD patients than in age-matched healthy subjects in vivo. In addition, the levels of midbrain [^{11}C](*R*)-PK11195 binding correlated negatively with the levels of [^{11}C]CFT binding in the putamen in the PD group. These results suggest that microglial activation was more significant in patients with more severe damage in the nigrostriatal pathway. This contention was supported by the results from the PD rat model showing the chronological decrease in [^{11}C]CFT accumulation in the lesioned striatum along with a parallel increase in [^{11}C](*R*)-PK11195 in the substantia nigra,[15] and from the postmortem analysis of the 1-methyl-4-phenyl-1,2,3,6-tetrahydropyridine–intoxicated human sub-

Table 3. Magnetic Resonance Imaging–based Midbrain Linear Measurements (cm), Mean (SD)[a]

Group	Antreroposterior Diameter	Interpeducular Distance
Parkinson's disease	26.5 (1.9)	36.8 (4.1)
Normal	27.6 (2.7)	37.4 (1.7)

There were no significant differences in measures between groups ($p > 0.05$, one-way analysis of variance).

[a]Results are maximum values of each distance.

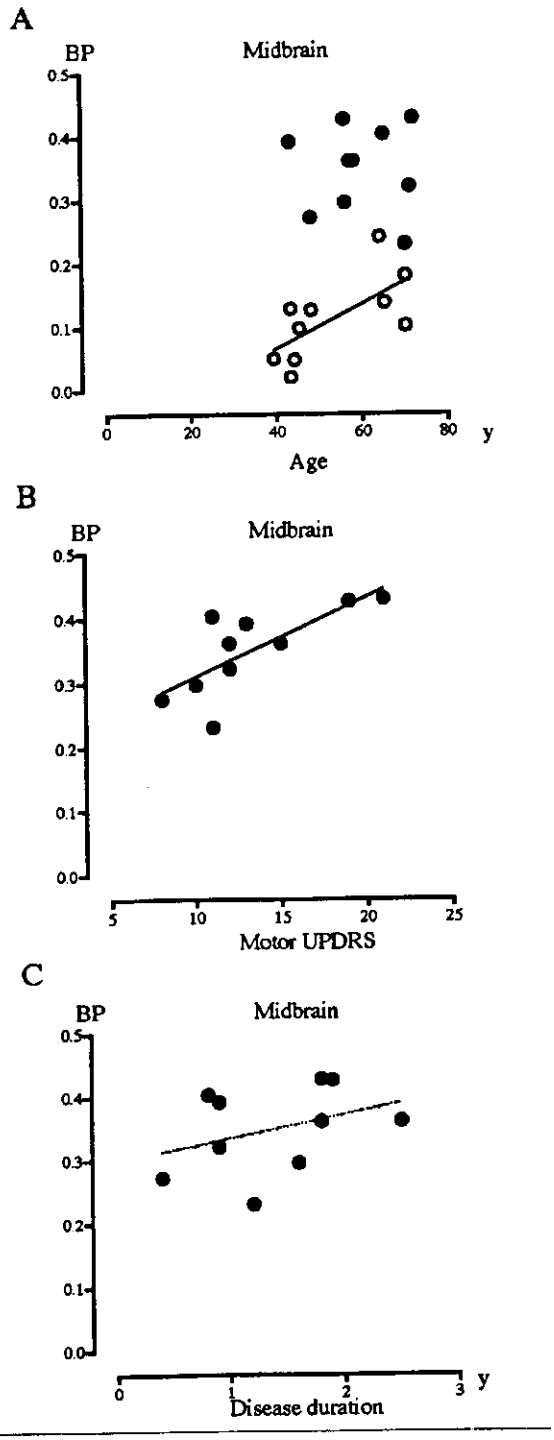

Fig 2. Correlations between levels of [^{11}C](R)-PK11195 binding in the midbrain and age (A) in the healthy group (open circles) *and Parkinson's disease group* (filled circles), *and motor scores of Unified Parkinson's Disease Rating Scale (UPDRS) (B), and disease duration (year) (C) in the Parkinson's disease group. BP = binding potential.*

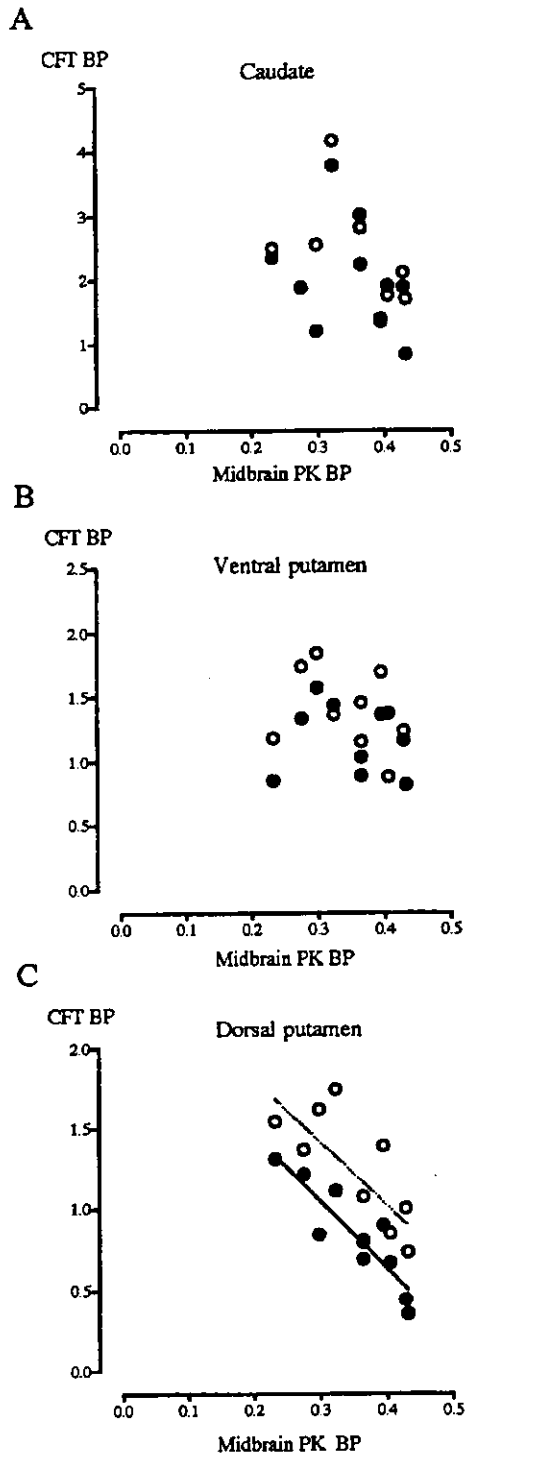

Fig 3. Correlations between levels of [^{11}C](R)-PK11195 binding potential (BP) in the midbrain and those of [^{11}C]CFT BP in the caudate (A), ventral putamen (B), and dorsal putamen (C) ipsilateral (open circles) *and contralateral* (filled circles) *to the clinically more affected side in the Parkinson's disease group.*

jects showing both elevated glial reaction in the substantia nigra and the dopaminergic neuronal loss.[10] Thus, our in vivo observation is compatible with the contention that microglial activation plays a key role in the initiation and progression of PD.

With respect to the role of microglia, there are lines of evidence that the majority of factors produced by activated microglia such as the cytokines tumor necrosis factor–α, interleukin-1β, and free radicals are proinflammatory or neurotoxic,[28–30] which suggests that activation of microglia would trigger the onset of a cascade of events resulting in a progressive degeneration of dopamine neurons. Although the age-related increase in [^{11}C](*R*)-PK11195 binding seen in healthy subjects in this study was not present in the PD group (see Fig 2A), it is likely that the degree of microglical activation associated with the disease is so great that it simply dwarfs the effect of aging. An age-related change in [^{11}C](*R*)-PK11195 binding in the thalamus in healthy subjects (data not shown) was also observed, as reported elsewhere.[16,31] These age-associated increases in microglial expression in the thalamus and midbrain may be related to the steady decline in higher cognitive and motor functions in normal aging that would jeopardize functional integration of the basal ganglia-cerebral cortical network. A lack of correlation of microglial activation with the disease duration (see Fig 2C) in this study suggested that the microglial reactive process might not be in parallel to the disease deterioration. To further illuminate this issue, this type of in vivo imaging on a chronological basis would be necessary.

There are a few methodological considerations to be noted in this study. First, PET has a critical limitation regarding image resolution for tiny structures such as the substantia nigra in the midbrain. A higher image resolution would enable us to elucidate the relation between microglial activation and dopaminergic neuronal loss in both nigrostriatal and mesolimbic (via the nucleus accumbens) systems by placing ROIs in those subregions of the midbrain. However, as shown in Figure 4, a greater degree of [^{11}C](*R*)-PK11195 binding tended to be observed in the midbrain contralateral to the clinically more affected side. Second, our tracer kinetic modeling was based on the reference tissue model,[26] and determination of normal reference tissue input was derived from the averaged value from the cerebral cortical regions in the 12 healthy subjects. Slightly lower levels of [^{11}C](*R*)-PK11195 binding in each of the brain regions examined in our study than the reported values[14,16] might be ascribed to the different methodological approach. However, the ratios of

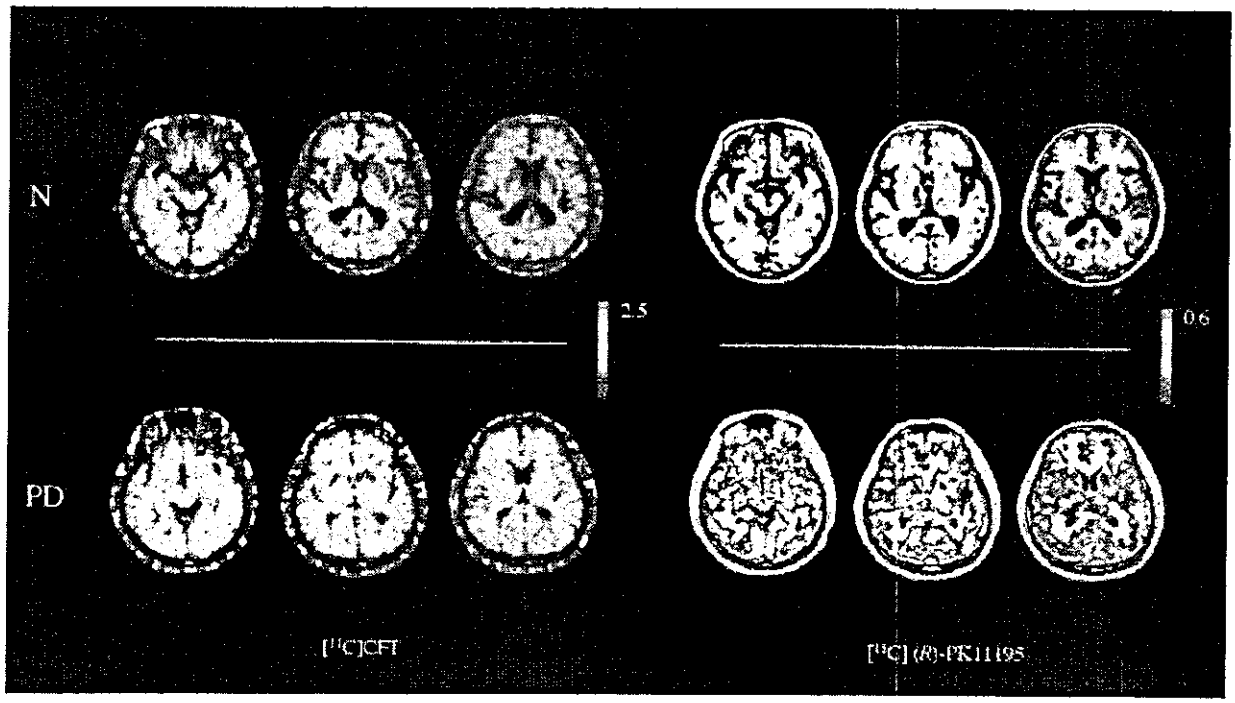

Fig 4. Magnetic resonance imaging positron emission tomography fusion parametric images of [^{11}C]CFT accumulation normalized to the cerebellum and [^{11}C](R)-PK11195 binding potential in a healthy subject (N) and a Parkinson's disease patient (PD) rated as Hoehn & Yahr stage 2. A marked increase in [^{11}C](R)-PK11195 binding was observed in the midbrain contralateral to the more disabled side along with a reduction in [^{11}C]CFT uptake in the putamen in the PD patient. For each tracer, red represents the highest value and dark violet represents the lowest value.

disease levels to control levels were fairly similar to those previously reported.

It has been reported that in PD, neuronal loss starts in the lateral ventral tier of the substantia nigra that projects to the dorsal putamen, and hence dopamine in the dorsal zone was more depleted than in the ventral zone in early PD.[1] This topological evidence supports our finding of a correlation between the increased [^{11}C](*R*)-PK11195 accumulation in the midbrain and the decreased accumulation of [^{11}C]CFT in the dorsal putamen (see Fig 3C). A more robust negative correlation was found clinically in the dorsal putamen contralateral to the more affected side. Interestingly, this nigral [^{11}C](*R*)-PK11195 accumulation was significantly correlated positively with motor severity in the present PD group (see Fig 2B). In contrast with the tegmental area or the medial tier of the substantia nigra projecting to the limbocortical region or the caudate (linking with mental and cognitive activities), because this dorsal putamen is considered to engage in motor execution,[32,33] this finding would reinforce the idea that the occurrence of microglial activation in the midbrain of PD at an early stage reflects dopamine loss sufficient to cause clinical parkinsonism.

From a therapeutic perspective, it was reported that antiinflammatory steroids,[34] nonsteroidal cyclooxygenase inhibitors,[35] and opioid receptor antagonist naloxone [36] might be promising as antiinflammatory agents for degenerative diseases such as PD. One epidemiological study agreed with the idea that use of nonsteroidal antiinflammatory drugs can delay the onset of PD.[37] In contrast, other clinical studies showed lesser effects of antiinflammatory drugs on a deceleration of the prevalence of PD than that in Alzheimer's disease[38,39] and therapeutic inconsistencies was suspected between laboratory data and clinical outcomes.[40] This result showing microglial activation along with dopaminergic terminal loss in vivo in early PD might afford a scope of discussion for use of the antiinflammatory and neuroprotective agents.

In conclusion, this study supports the contention that microglial activation develops in the midbrain of PD patients at an early stage, and that this appearance may be associated with likely ensuing apoptotic events. The latter issue must be clarified by a chronological study, but the present, one-time, double-tracer study for targeting both neuroinflammation and neuronal loss in the nigrostriatal system provides essential information about the degeneration process in PD.

We thank all patients and healthy subjects who participated in this study, Dr K. Tanaka and Dr M. Sakamoto for patients' selection, H. Okada for his constant technical support, Dr Y. Magata for his valuable advice on radiocompound syntheses, and our staff for support of the present PET study.

References

1. Kish SJ, Shannak K, Hornykiewicz O. Uneven pattern of dopamine loss in the striatum of patients with idiopathic Parkinson's disease. Pathophysiologic and clinical implications. N Engl J Med 1988;318:876–880.
2. McGeer PL, Itagaki S, Akiyama H, McGeer EG. Rate of cell death in parkinsonism indicates active neuropathological process. Ann Neurol 1988;24:574–576.
3. McGeer PL, Itagaki S, Boyes BE, McGeer EG. Reactive microglia are positive for HLA-DR in the substantia nigra of Parkinson's and Alzheimer's disease brains. Neurology 1988;38: 1285–1291.
4. Mirza B, Hadberg H, Thomsen P, Moos T. The absence of reactive astrocytosis is indicative of a unique inflammatory process in Parkinson's disease. Neuroscience 2000;95:425–432.
5. Vila M, Jackson-Lewis V, Guegan C, et al. The role of glial cells in Parkinson's disease. Curr Opin Neurol 2001;14: 483–489.
6. Akiyama H, McGeer PL. Microglial response to 6-hydroxydopamine-induced substantia nigra lesions. Brain Res 1989; 489:247–253.
7. Gao HM, Jiang J, Wilson B, et al. Microglial activation-mediated delayed and progressive degeneration of rat nigral dopaminergic neurons: relevance to Parkinson's disease. J Neurochem 2002;81:1285–1297.
8. Sherer TB, Betarbet R, Kim JH, Greenamyre JT. Selective microglial activation in the rat rotenone model of Parkinson's disease. Neurosci Lett 2003;341:87–90.
9. Sugama S, Yang L, Cho BP, et al. Age-related microglial activation in 1-methyl-4-phenyl-1,2,3,6-tetrahydropyridine (MPTP)-induced dopaminergic neurodegeneration in C57BL/6 mice. Brain Res 2003;964:288–294.
10. Langston JW, Forno LS, Tetrud J, et al. Evidence of active nerve cell degeneration in the substantia nigra of humans years after 1-methyl-4-phenyl-1,2,3,6 tetrahydropyridine exposure. Ann Neurol 1999;46:598–605.
11. McGeer PL, Schwab C, Parent A, Doudet D. Presence of reactive microglia in monkey substantia nigra years after 1-methyl-4-phenyl-1,2,3,6-tetrahydropyridine administration. Ann Neurol 2003;54:599–604.
12. Kreutzberg GW. Microglia: a sensor for pathological events in the CNS. Trends Neurosci 1996;19:312–318.
13. Conway EL, Gundlach AL, Craven JA. Temporal changes in glial fibrillary acidic protein messenger RNA and [3H]PK11195 binding in relation to imidazoline-I2-receptor and alpha 2-adrenoceptor binding in the hippocampus following transient global forebrain ischaemia in the rat. Neuroscience 1998;82: 805–817.
14. Banati RB, Newcombe J, Gunn RN, et al. The peripheral benzodiazepine binding site in the brain in multiple sclerosis: quantitative in vivo imaging of microglia as a measure of disease activity. Brain 2000;123:2321–2337.
15. Cicchetti F, Brownell AL, Williams K, et al. Neuroinflammation of the nigrostriatal pathway during progressive 6-OHDA dopamine degeneration in rats monitored by immunohistochemistry and PET imaging. Eur J Neurosci 2002;15:991–998.
16. Cagnin A, Brooks DJ, Kennedy AM, et al. In-vivo measurement of activated microglia in dementia. Lancet 2001;358: 461–467.
17. Banati RB. Visualising microglial activation in vivo. Glia 2002; 40:206–217.
18. Frost JJ, Rosier AJ, Reich SG, et al. Positron emission tomographic imaging of the dopamine transporter with 11C-WIN 35,428 reveals marked declines in mild Parkinson's disease. Ann Neurol 1993;34:423–431.

19. Wullner U, Pakzaban P, Brownell AL, et al. Dopamine terminal loss and onset of motor symptoms in MPTP-treated monkeys: a positron emission tomography study with 11C-CFT. Exp Neurol 1994;126:305–309.
20. Ouchi Y, Yoshikawa E, Okada H, et al. Alterations in binding site density of dopamine transporter in the striatum, orbitofrontal cortex, and amygdala in early Parkinson's disease: compartment analysis for beta-CFT binding with positron emission tomography. Ann Neurol 1999;45:601–610.
21. Watanabe M, Shimizu K, Omura T, et al. A new high resolution PET scanner dedicated to brain research. IEEE Trans Nucl Sci 2002;49:634–639.
22. Wong DF, Yung B, Dannals RF, et al. In vivo imaging of baboon and human dopamine transporters by positron emission tomography using [11C]WIN 35,428. Synapse 1993;15: 130–142.
23. Doraiswamy PM, Na C, Husain MM, et al. Morphometric changes of the human midbrain with normal aging: MR and stereologic findings. AJNR Am J Neuroradiol 1992;13: 383–386.
24. Mai JK, Assheuer J, Paxinos G. Atlas of the human brain. San Diego: Academic Press, 1997.
25. Ouchi Y, Kanno T, Okada H, et al. Presynaptic and postsynaptic dopaminergic binding densities in the nigrostriatal and mesocortical systems in early Parkinson's disease: a double-tracer positron emission tomography study. Ann Neurol 1999; 46:723–731.
26. Lammertsma AA, Bench CJ, Hume SP, et al. Comparison of methods for analysis of clinical [11C]raclopride studies. J Cereb Blood Flow Metab 1996;16:42–52.
27. Gun R, Lammertsma AA, Cunningham VJ. Parametric imaging of ligand-receptor binding in PET using a simplified reference tissue model and cluster analysis. In: Carson R, Daule M, Witherspoon P, Herscovitch P, eds. Quantitative functional brain imaging with PET. San Diego, CA: Academic Press, 1998:401–406.
28. Boje KM, Arora PK. Microglial-produced nitric oxide and reactive nitrogen oxides mediate neuronal cell death. Brain Res 1992;587:250–256.
29. Ehrlich LC, Hu S, Sheng WS, et al. Cytokine regulation of human microglial cell IL-8 production. J Immunol 1998;160: 1944–1948.
30. McGuire SO, Ling ZD, Lipton JW, et al. Tumor necrosis factor alpha is toxic to embryonic mesencephalic dopamine neurons. Exp Neurol 2001;169:219–230.
31. Banati RB, Cagnin A, Brooks DJ, et al. Long-term trans-synaptic glial responses in the human thalamus after peripheral nerve injury. Neuroreport 2001;12:3439–3442.
32. Ouchi Y, Yoshikawa E, Futatsubashi M, et al. Effect of simple motor performance on regional dopamine release in the striatum in parkinson disease patients and healthy subjects: a positron emission tomography study. J Cereb Blood Flow Metab 2002;22:746–752.
33. Goerendt IK, Messa C, Lawrence AD, et al. Dopamine release during sequential finger movements in health and Parkinson's disease: a PET study. Brain 2003;126:312–325.
34. Castano A, Herrera AJ, Cano J, Machado A. The degenerative effect of a single intranigral injection of LPS on the dopaminergic system is prevented by dexamethasone, and not mimicked by rh-TNF-alpha, IL-1beta and IFN-gamma. J Neurochem 2002;81:150–157.
35. Lipsky PE. The clinical potential of cyclooxygenase-2-specific inhibitors. Am J Med 1999;106:51S–57S.
36. Liu B, Hong JS. Role of microglia in inflammation-mediated neurodegenerative diseases: mechanisms and strategies for therapeutic intervention. J Pharmacol Exp Ther 2003;304:1–7.
37. Chen H, Zhang SM, Hernan MA, et al. Nonsteroidal anti-inflammatory drugs and the risk of Parkinson disease. Arch Neurol 2003;60:1059–1064.
38. McGeer PL, Schulzer M, McGeer EG. Arthritis and anti-inflammatory agents as possible protective factors for Alzheimer's disease: a review of 17 epidemiologic studies. Neurology 1996;47:425–432.
39. Czlonkowska A, Kurkowska-Jastrzebska I, Czlonkowski A, et al. Immune processes in the pathogenesis of Parkinson's disease—a potential role for microglia and nitric oxide. Med Sci Monit 2002;8:RA165–RA177.
40. Schapira AH, Olanow CW. Neuroprotection in Parkinson disease: mysteries, myths, and misconceptions. JAMA 2004; 291:358–364.

Neuropsychopharmacology (2004) 29, 1019–1026

www.neuropsychopharmacology.org

Metabolite Alterations in Basal Ganglia Associated with Psychiatric Symptoms of Abstinent Toluene Users: A Proton MRS Study

Kiyokazu Takebayashi[1], Yoshimoto Sekine[1], Nori Takei*[1,2,3], Yoshio Minabe[1], Haruo Isoda[4], Hiroyasu Takeda[4], Katsuhiko Nishimura[1], Kazuhiko Nakamura[1], Katsuaki Suzuki[1], Yasuhide Iwata[1], Harumi Sakahara[4] and Norio Mori[1]

[1]Department of Psychiatry and Neurology, Hamamatsu University School of Medicine, Hamamatsu, Shizuoka, Japan; [2]Stanley Foundation Research Center in Japan, Hamamatsu, Shizuoka, Japan; [3]Department of Psychological Medicine, Institute of Psychiatry, London, UK; [4]Department of Radiology, Hamamatsu University School of Medicine, Hamamatsu, Shizuoka, Japan

Long-term toluene abuse causes a variety of psychiatric symptoms. However, little is known about abnormalities at the neurochemical level in the living human brain after long-term exposure to toluene. To detect neurochemical changes in the basal ganglia of subjects with a history of long-term toluene use, proton magnetic resonance spectroscopy (^{1}H MRS) was performed in 12 abstinent toluene users and 13 healthy comparisons with no history of drug abuse. *N*-acetylaspartate (NAA), creatine plus phosphocreatine (Cr + PCr), choline-containing compounds (Cho), and myo-inositol (MI) levels were measured in the left and right basal ganglia. The Cho/Cr + PCr ratio, a marker of membrane metabolism, was significantly increased in the basal ganglia of toluene users in comparison to that of the control subjects. Furthermore, the increase in the Cho/Cr + PCr ratio was significantly correlated with the severity of residual psychiatric symptoms. These findings suggest that long-term toluene use causes membrane disturbance in the basal ganglia, which is associated with residual psychiatric symptoms that persist even after long-term abstinence from toluene use.
Neuropsychopharmacology (2004) **29,** 1019–1026, advance online publication, 24 March 2004; doi:10.1038/sj.npp.1300426

Keywords: toluene-related symptoms; proton magnetic resonance spectroscopy; basal ganglia

INTRODUCTION

Organic solvent abuse is a worldwide problem, particularly among adolescents (Flanagan and Ives, 1994; Neumark *et al*, 1998). The easy accessibility to organic solvents makes them among the first drugs tried by teenagers. Consequently, teenagers are liable to develop an addiction to organic solvents, and such use can serve as a 'gateway' to the ingestion of other illicit drugs (Ives, 2000). Toluene is one of the major components of many organic solvents and is highly lipid-soluble (Morton, 1987). Toluene rapidly permeates lipid-rich regions of the body such as the brain, and its recreational intake can cause chronic and persistent psychiatric symptoms, including hallucinations and alterations in personality, even after cessation of toluene use (Hormes *et al*, 1986; Morton, 1987). However, the mechanisms responsible for these residual psychiatric symptoms following chronic toluene use remain unknown.

In experimental animal studies, exposure to toluene has been shown to produce changes in lipid membrane fluidity and membrane function (Kyrklund *et al*, 1987; LeBel and Schatz, 1990; von Euler *et al*, 1990). Furthermore, long-term exposure to toluene induces a persistent dopaminergic dysfunction in the rat basal ganglia, and this toluene-induced dopaminergic dysfunction has been related to the behavioral changes and the persistent cognitive deficits in rats (Cintra *et al*, 1999; Hillefors-Berglund *et al*, 1995; von Euler *et al*, 1993, 2000).

In human MR studies of toluene users, T2-weighted magnetic resonance images revealed global atrophy in the cerebrum, cerebellum, and brainstem (Rosenberg *et al*, 1988). Loss of differentiation between gray and white matter, increased periventricular white matter signal intensity (Aydin *et al*, 2002; Filley *et al*, 1990; Rosenberg *et al*, 1988, 2002), and hypointensity in the thalamus and

*Correspondence: Dr N Takei, Department of Psychiatry and Neurology, Hamamatsu University School of Medicine, 1-20-1 Handayama, Hamamatsu, 431-3192 Shizuoka, Japan, Tel: +81 53 435 2295, Fax: +81 53 435 3621,
E-mail address: ntakei@hama-med.ac.jp
Received 04 August 2003; revised 23 January 2004; accepted 27 January 2004
Online publication: 5 February 2004 at http://www.acnp.org/citations/Npp02050403349/default.pdf

basal ganglia (Rosenberg *et al*, 2002; Unger *et al*, 1994) have also been found in toluene users. Furthermore, white matter changes have been reported to be associated with neurocognitive deficits in long-term toluene users (Filley *et al*, 1990). However, little is known about the effects of long-term toluene use on the human brain at the neurochemical level.

Proton magnetic resonance spectroscopy (^{1}H MRS) offers an opportunity to evaluate *in vivo* neurochemical changes that might occur in toluene users. In this study, we investigated the potential of ^{1}H MRS scanning for revealing neurochemical changes in the chemistry of the basal ganglia of abstinent toluene users; we also considered whether or not such changes, if found, could possibly be related to the clinical characteristics observed in abstinent toluene users.

METHODS

Subjects

A total of 12 toluene users and 13 healthy comparison subjects who had never used toluene were recruited for our comprehensive research project on substance-related psychiatric disorders. Candidates were excluded if they were seropositive for human immunodeficiency virus type-1 (HIV-1), if they had a history of head trauma with loss of consciousness, or if they had brain morphological abnormalities (eg atrophy or tumor, etc) on MR images. All participants showed no neurological abnormalities and had no history of stupor or coma, which may be observed during intoxication after the use of high doses of toluene. All subjects were screened using the Structured Clinical Interview for DSM-IV (SCID) (First *et al*, 1996). More specifically, detailed information on toluene use and the history of psychiatric symptoms was retrospectively obtained from the toluene users; SCID-based interviews with the users and their family members were conducted, and patient medical records were considered as well. None of the toluene users had used any other drugs (ie they were mono-drug users) and the subjects had had no history of DSM-IV mental disorders before the use of toluene. The comparison subjects had no experience of the use of any illicit drugs, and had no history of mental disorders, including substance-related disorders, according to the DSM-IV. Both groups reported similar occasional smoking and drinking habits, and none of the subjects matched the DSM-IV criteria for either nicotine- or the alcohol-related disorders. The toluene users were recruited from the Hamamatsu University Hospital, and from three associated hospitals (Hattori Mental Hospital, Shimada Municipal Hospital, and Hamamatsu Neurological Hospital).

The duration of toluene use was defined as the time that had intervened between the initial and the last use of toluene. In cases involving intervals of abstinence exceeding 1 month during the duration of toluene use as defined, these intervals were subtracted from the total length of toluene use. The duration of abstinence from toluene use was defined as the time between the day of the last use of toluene and the day of the ^{1}H MRS examination. Cumulative lifetime exposure to toluene was estimated in milliliters. Among the 12 toluene users, five had been treated with neuroleptics, while the remaining seven toluene users had not previously taken neuroleptics prior to the ^{1}H MRS examination. Current and total lifetime neuroleptic doses in the five toluene users were quantified in chlorpromazine-equivalent dosages (American Psychiatric Association, 1997). In order to establish recent abstinence from toluene use, we regularly tested the subjects for urinary hippuric acid, a biomarker of toluene use (Raikhlin-Eisenkraft *et al*, 2001), using high-performance liquid chromatography, which was carried out according to the standard diagnostic methods. In addition, to verify abstinence from other illicit drugs, we used a rapid immunoassay for the qualitative detection of the metabolites of the following eight classes of drugs: amphetamines (including (±)3,4-methylenedioxymethamphetamine and methamphetamine), barbiturates, benzodiazepines, cocaine, methadone, opiates, tetrahydrocannabinol, and tricyclic antidepressants (Triage 8, Biosite Diagnostics, San Diego, USA). These assessments were also performed on the same day as the ^{1}H MRS examination. Psychiatric symptoms in the toluene users were evaluated using the Brief Psychiatric Rating Scale (BPRS) (Overall and Gorham, 1962) on the day of the ^{1}H MRS study. The assessment was conducted by a trained research psychiatrist blind to the ^{1}H MRS data. After providing the subjects with a complete description of the study, written informed consent was obtained from all participants before entry into the study, in compliance with the procedures of the Ethics Committee of the Hamamatsu University School of Medicine.

Image Acquisition

MRS was performed at the Hamamatsu University Hospital, using a 1.5-T whole-body MR scanner (Signa Horizon; General Electric Medical Systems, Milwaukee, WI, USA) equipped with self-shielded gradient coils. A quadrature, MR bird-cage coil (trans/receive) was used throughout the study. The localized MR spectra were recorded using the point-resolved spatially localized spectroscopy (PRESS) sequence from the bilateral basal ganglia. The RF transmitter frequency was centered at the water resonance frequency (63.88 MHz). A 90° flip angle was determined by varying the RF amplifier gain until a maximal signal consistent with a good slice profile was obtained. The B_0 shim on the 27 ml cubic excited volume was optimized using linear shims to a full-width at half-maximum (FWHM) of <6.4 Hz. Voxel size was 8 cm^3 ($2 \times 2 \times 2$ cm^3). To establish the voxel of interest (VOI) on an MR image, scout views in the proton density images were obtained vertically in the *Z*-axis (Figure 1). Proton density images were acquired because gray matter contrasts well with white matter in this type of imaging study (Sekine *et al*, 2002).

After the location of the VOI had been verified by localized MR imaging, the magnetic field in the VOI was optimized by means of a water signal to establish a linewidth of <3 Hz. The acquisition parameters were as follows: repetition time (TR), 1500 ms; echo time (TE), 40 ms; and acquisition time, 3 min 42 s. Peaks of *N*-acetylaspartate (NAA) (2.0 ppm), creatine plus phosphocreatine (Cr + PCr) (3.0 ppm), choline-containing compounds (Cho) (3.2 ppm), and myo-inositol (MI) (3.6 ppm) were obtained. Data processing were performed using a PROBE/SV-Quant tool (General Electric Medical Systems,